

Designing of Thiophene [3, 2-b] Pyrrole Ring-Based NFAs for High-Performance Electron Transport Materials: A DFT Study

Sahar Javaid Akram, N. M. A. Hadia, Ahmed M. Shawky, Javed Iqbal,* Muhammad Imran Khan, Naifa S. Alatawi, Mahmoud A. A. Ibrahim, Muhammad Ans, and Rasheed Ahmad Khara*



Cite This: *ACS Omega* 2023, 8, 11118–11137



Read Online

ACCESS |



Metrics & More

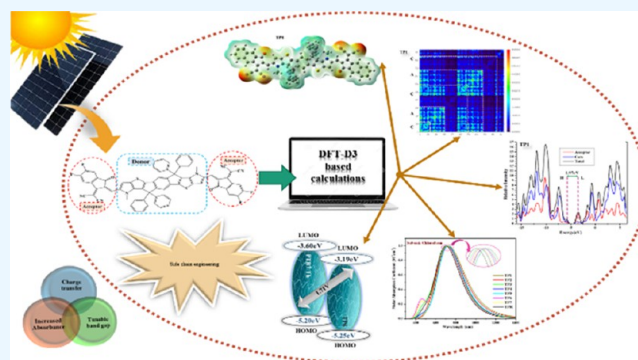


Article Recommendations



Supporting Information

ABSTRACT: Among the blended components of a photoactive layer in organic photovoltaic (OPV) cells, the acceptor is of high importance. This importance is attributed to its increased ability to withdraw electrons toward itself for their effective transport toward the respective electrode. In this research work, seven new non-fullerene acceptors were designed for their possible utilization in the OPVs. These molecules were designed through side-chain engineering of the PTBTP-4F molecule, with its fused pyrrole ring-based donor core and different strongly electron-withdrawing acceptors. To elucidate their effectiveness, the band gaps, absorption characteristics, chemical reactivity indices, and photovoltaic parameters of all of the architecture molecules were compared with the reference. Through various computational software, transition density matrices, graphs of absorption, and density of states were also plotted for these molecules. From some chemical reactivity indices and electron mobility values, it was proposed that our newly designed molecules could be better electron-transporting materials than the reference. Among all, TP1, due to its most stabilized frontier molecular orbitals, lowest band gap and excitation energies, highest absorption maxima in both the solvent and gas medium, least hardness, highest ionization potential, superior electron affinity, lowest electron reorganization energy, as well as highest rate constant of charge hopping, seemed to be the best molecule in terms of its electron-withdrawing abilities in the photoactive layer blend. In addition, in terms of all of the photovoltaic parameters, TP4–TP7 was perceived to be better suited in comparison to TPR. Thus, all our suggested molecules could act as superior acceptors to TPR.



1. INTRODUCTION

With the rapid surge in population and development of the global economy, the demand for energy sources alternative to the pollution-causing nonrenewable ones has been increasing tremendously. Among the different renewable energy resources, the most eco-friendly and carbon-neutral one seems to be solar energy.¹ This inexhaustible energy supply appears to be the most reliable, affordable, and clean option available out there. This energy from the sun has been converted into a valuable electrical one, for decades, with the help of silicon-based inorganic solar cells. But despite their high photo-to-electric conversion efficiency (PCE), the large-scale application of silicon solar cells seems to be limited due to their shortcomings, such as being expensive, heavy, and bearing an inflexible morphology.² Subsequently, a leapfrog development in the field of photovoltaics has been seen in the organic counterparts of silicon solar cells. Organic photovoltaic cells have been made virtually practical due to their potentially low-cost solution processability, the mechanical stability of the active layer, high semi-transparency, flexibility, as well as structurally tunable electronic and absorption properties.³

In organic photovoltaic cells, it is imperative for the photoactive layer to have an appropriate morphology and light-absorbing molecules. In this regard, bulk heterojunction has proved itself to be quite proficient due to some multifarious non-fullerene acceptors (NFAs).⁴ Actually, in the BHJ formation of a photoactive layer, the donor and acceptor materials are intermixed in such a way that they reduce the chances of recombination between the generated excitons. The excitons are those closely coupled electron–hole pairs that have to dissociate into separate charge-transfer states, and this separation of electron and hole pair occurs at the interface between the two distinct polymer donor and acceptor layers, which is highly facilitated by BHJs.⁵

Received: December 14, 2022

Accepted: March 8, 2023

Published: March 17, 2023



Formerly, the acceptor layer in BHJs was once the most extensively used and highly electron-withdrawing PC₆₁BM and PC₇₁BM molecules. Though they remained unbeatable for quite a lengthy period, their limited absorption in the visible and infrared spectrum, low structural flexibility, fixed morphology, and poor photostability, in addition to their high synthetic cost, increased the popularity of their counterparts, the non-fullerene acceptors (NFAs).⁶ The NFAs have made up for the limitations of fullerene acceptors due to their strong absorption and light-harvesting capability in the visible and near IR regions, easy and affordable synthesis, flexible frontier molecular orbitals (FMOs), enhanced thermal stability, and highly versatile molecular structure.⁷ In addition, they have made it possible for organic photovoltaics to reach a PCE of around 19% with apt polymer donors when only 11% is possible with their fullerene equivalents.⁸ Likewise, due to their structurally tunable electrochemical properties, NFA series, such as ITIC and Y6, have replaced fullerene acceptors revolutionarily and could attain greater PCE by the introduction of more electron-withdrawing and conjugated moieties at their peripheries.⁹

In this research work, a pyrrole-based NFA, PTBTP-4F (TPR), has been structurally modified by substitution of its end-capped electron-withdrawing 2-(5,6-difluoro-2-methylene-3-oxo-indan-1-yl)-malononitrile acceptor moieties with seven different significantly electron-withdrawing or conjugated peripheral acceptors. The core of this IDT (indacenodithiophene)-fused pyrrole (TP)-based A–D–A type molecule, due to its strong electron-donating nitrogen atom on the top of red-shifting absorption maxima, facilitates higher energy levels and provides an extra reactive site to the molecule. The optical band gap of this molecule was also seen to be only 2.08 eV due to its high intramolecular charge transfer and molecular stacking, which could be endorsed by its highly conjugated donor core. Furthermore, PTBTP-4F, while having relatively low V_{OC} , showed a high short-circuit current density of 20.74 mA cm⁻², an absorption range of 500–900 nm in the chloroform solvent, and a tremendous PCE of 12.33%.¹⁰ Therefore, to utilize the promising core of this molecule, seven new molecules were designed through its side-chain manipulation to introduce high-performance NFAs having increased open-circuit photovoltage, in addition to being highly effective in the photoactive layers of the corresponding OPVs.

Precisely, in the present work, the newly generated molecules had a TP donor core and seven different acceptors such as 1-dicyanomethylene-2-methylene-3-oxo-indan-5,6-dicarbonitrile (TP1), 6-cyano-3-dicyanomethylene-2-methylene-1-oxo-indan-5-carboxylic acid methyl ester (TP2), 1-dicyanomethylene-2-methylene-3-oxo-indan-5,6-dicarboxylic acid dimethyl ester (TP3), 2-(2-methylene-3-oxo-2,3-dihydro-cyclopenta[*b*]naphthalen-1-ylidene)-malononitrile (TP4), 2-(6,7-difluoro-2-methylene-3-oxo-2,3-dihydro-cyclopenta[*b*]naphthalen-1-ylidene)-malononitrile (TP5), 2-(5-methylene-1-methylsulfanyl-6-oxo-5,6-dihydro-cyclopenta[*c*]thiophen-4-ylidene)-malononitrile (TP6), and 2-(1-chloro-5-methylene-6-oxo-5,6-dihydro-cyclopenta[*c*]thiophen-4-ylidene)-malononitrile (TP7). The optical, photophysical, and electronic along with the morphological properties of all of the TP1–TP7 molecules, were studied and compared with the reference TPR to analyze their prospective capabilities in the photoactive BHJ layer of OPVs.

2. COMPUTATIONAL METHODOLOGY

Density functional theory (DFT)¹¹ and its time-dependent approach (TD-DFT)¹² are both known to be one of the most reliable and prominently widespread theoretical methods to study the correspondence between geometry and optoelectronic aspects of any molecule. Here, we used the dispersion-corrected DFT-D3 wide-accepted variant of this approach. Before performing any computational calculations, the designs of the molecules were sketched using ChemDraw 7.0 software.¹³ Using all of these sketches, the computational calculations were performed through the Gaussian 09 set of programs. Therefore, to evaluate the reliability of any one level of theory among the different ones in the DFT, the four most common functionals from Gaussian software¹⁴ were analyzed concerning the reference molecule (TPR). After cross-examination of the band gaps at the ground state and absorption maxima in the chloroform solvent phase (using a polarizable continuum model¹⁵) of all of the four functionals with their experimental values, the B3LYP functional was perceived to be the most precise one to the experimental results and thus was selected as the method of computation.

After the careful designation of the functional, the molecules of study were optimized at the ground state (with D3 dispersion taken into account) to comprehend their molecular electrostatic potentials (MEPs), as well as frontier molecular orbitals (FMOs) and related band gaps. The results of the FMO evaluation were verified with the help of the peaks of the density of states, plotted using the PyMOlyze 1.1 program.¹⁶ This density of states actually determine the possibility of the existence of an electron in any specific energy level of the molecule and also help in evaluating the contribution of either donor or acceptor fragment of the molecules in raising the highest occupied molecular orbital (HOMO) or the lowest unoccupied molecular orbital (LUMO).

Moreover, for the excited phase calculations of the molecules, their excitation energies, oscillator strengths, electron dissociation energies, dipole moments, and light-harvesting efficiencies were computed in the gaseous phase, in addition to the chloroform solvent medium. Additionally, for the sake of evaluation of the wavelengths of maximum absorption (λ_{max}) in both these mediums, the absorption graphs of all of the molecules were plotted and studied using Origin 6.0 software.¹⁷ Then, to study the chemical reactivity of the molecules, some chemical reactivity indices, such as ionization potential, chemical softness, etc., were calculated using the energies of the anions, cations, and neutral states of the molecules. Moreover, the transition density matrices of the two fragments of the molecules were plotted through two-dimensional maps using Multiwfn 3.7 software.¹⁸ From these maps, the charge localization, as well as delocalization probabilities, within the structures were effortlessly understood.

Furthermore, in a quest to analyze the charge mobility of the studied molecules, the rate constant for charge hopping was taken into account with the help of Marcus theory. According to this theory, the rate constant for charge hopping (k) has a direct correspondence with the charge-transfer integral and an inverse one with the reorganization energies of the hole and electron (eq 1).¹⁹

$$k = t^2 \sqrt{\frac{\pi}{h^2 k_B T \lambda}} \exp\left[-\frac{\lambda}{4k_B T}\right] \quad (1)$$

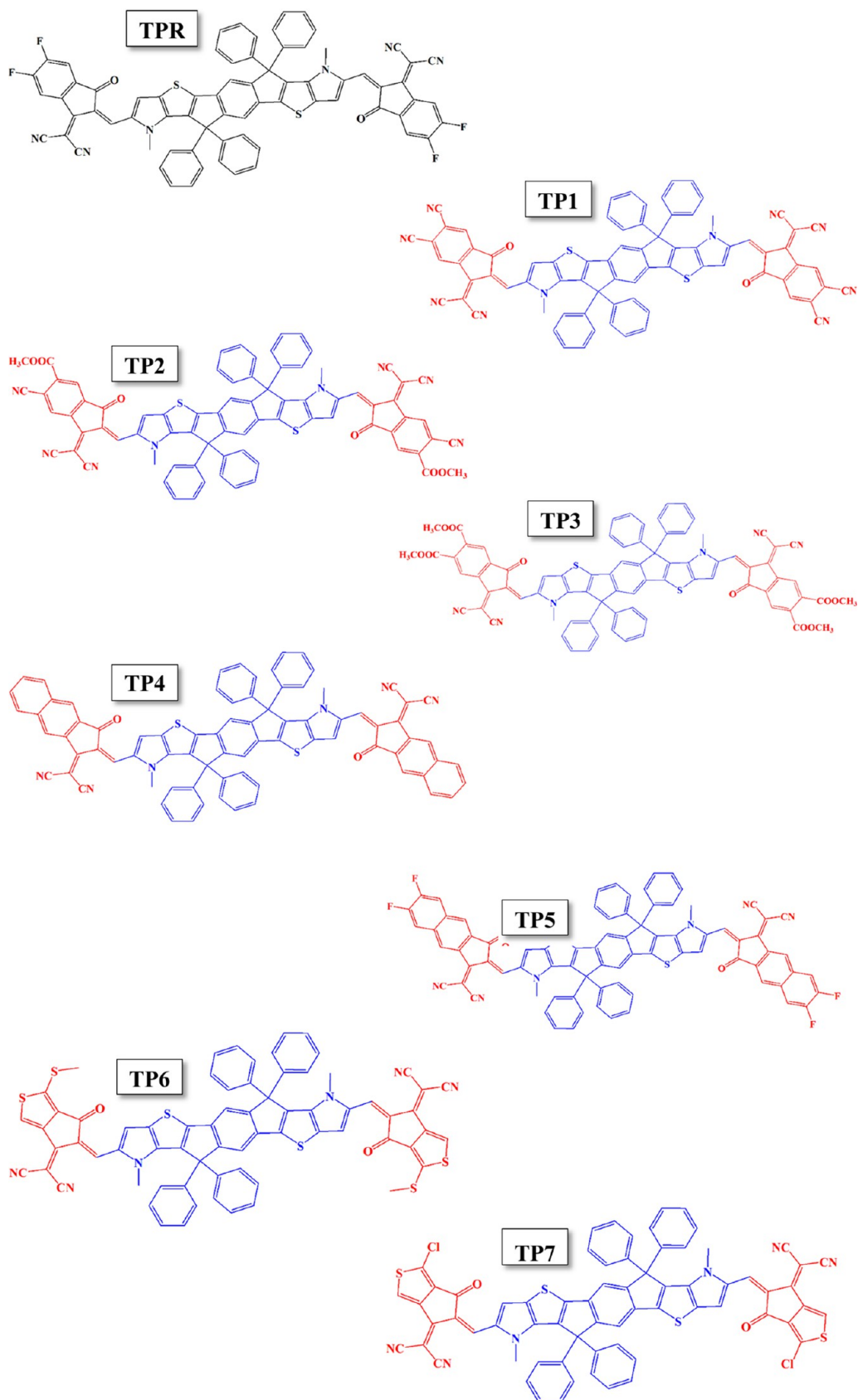


Figure 1. Molecular sketches of the molecules drawn using ChemDraw (blue = core, red = acceptors, and black as whole = reference).

Here, k_B and h are Boltzmann's and Planck's constants, respectively. T is the absolute temperature of 298 K in this study, t is the charge-transfer integral of electron (t_{electron}) and

hole (t_{hole}), and finally, the term " λ " represents the reorganization energies of either hole (λ_{hole}) or electron ($\lambda_{\text{electron}}$).²⁰

Taking the values of the charge hopping integral into account, it was anticipated that our derived molecules might act as proficient acceptors in the assortment of the photoactive layer. Thus, the open-circuit photovoltage and the fill factor of all of the analyzed acceptors were computed with respect to the common donor molecule “PTB7-Th”.²¹ The values of these photovoltaic parameters, in addition to the light-harvesting efficiency, helped us to have a rough estimate of the best possible candidature of the designed acceptors for their futuristic applications in OPVs’ photoactive layer. The sketch of all molecules are depicted in (Figure 1).

3. RESULTS AND DISCUSSIONS

3.1. Method of Selection. For the selection of the most accurate and consistent method of computation intended for this research work, the results of four different functionals were examined with the experimental ones of the reference molecule (TPR). These functionals are quite frequently used because of their effectiveness in theoretical works, namely, B3LYP,²² CAM-B3LYP,²³ MPW1PW91,²⁴ and wB97XD.²⁵ With these four functionals at the 6-31G(d,p)²⁶ level of theory, ground state optimization and excited state calculations of the reference molecule were executed. At the ground state, the frontier molecular orbitals and the corresponding band gaps of all of the functionals were compared with the experimentally computed numerical values of TPR. From the compiled data of the FMOs in Table 1, it is clear that the B3LYP functional

Table 1. Compared Frontier Molecular Orbitals and Band Gap of Four Analyzed Functionals with the Experimental Values

method	HOMO	LUMO	band gap
experimental	-5.39	-3.31	2.08
B3LYP	-5.39	-3.30	2.09
CAM-B3LYP	-6.44	-2.28	4.16
MPW1PW91	-5.63	-3.29	2.34
WB97XD	-7.01	-1.80	5.21

significantly reproduced the experimental values for the reference molecule. Then, in the pursuance of validation of the functionality of the B3LYP functional in the excited state, the experimental wavelength of maximum absorption (λ_{max}) of TPR in chloroform (732 nm) was paralleled to that of the ones attained from all of the four analyzed functionals (Figure 2).¹⁰ Even in this case, B3LYP (706 nm) functional seemed to be the most profound one and thus was selected as the functional of our study. Additionally, with this selected functional, D3 dispersion was taken into account for all further studies, as it analyzes the dispersion energies during any calculations²⁷ and has proved itself to do well in reproducing the experimental trends.²⁸

3.2. Design of the Molecules and Their Geometric Properties. The molecules were designed through the substitution of various acceptor molecules in the reference TPR. These specific acceptors were utilized due to their strong electron-withdrawing capabilities and significant effect on the optical, electronic, morphological, and photovoltaic aspects of the overall molecule in the previously reported literature. Additionally, the first three substituted acceptor groups (in TP1–TP3) differ from the reference molecule only with respect to the peripheral functional groups, i.e., cyano (–CN) and acetyl (–COOCH₃) instead of the fluoro groups. These –CN and –COOCH₃ groups were utilized due to their increased unsaturation not being present in the fluoro of TPR.²⁹ Furthermore, the acceptors of the next two molecules TP4 and TP5 had an additional phenyl ring from the others, and between these two, the only difference was fluoro atoms; this way, their varying behavior from the reference and between themselves could be effectively studied. Similar is the case with the remaining two molecules. Additionally, the point of substitution of these acceptor groups was retained just as the one in the reference molecule so that only the effect of varying acceptors could be studied without the hindrance of the substitution position (another vast topic in the field of OPVs).³⁰

To appraise the consequence of side-chain manipulation on the geometry of the molecule, all of the molecular structures

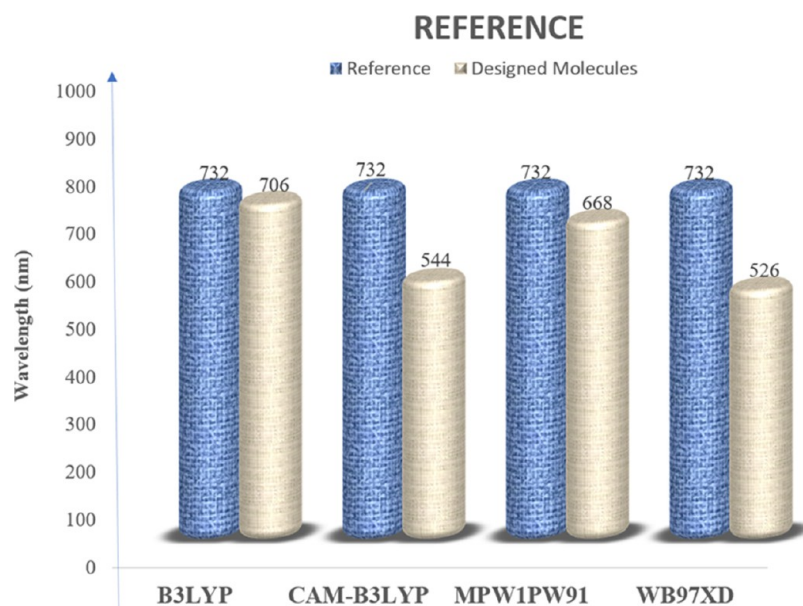


Figure 2. Compared λ_{max} of all of the functionals with the experimental λ_{max} of 706 nm.

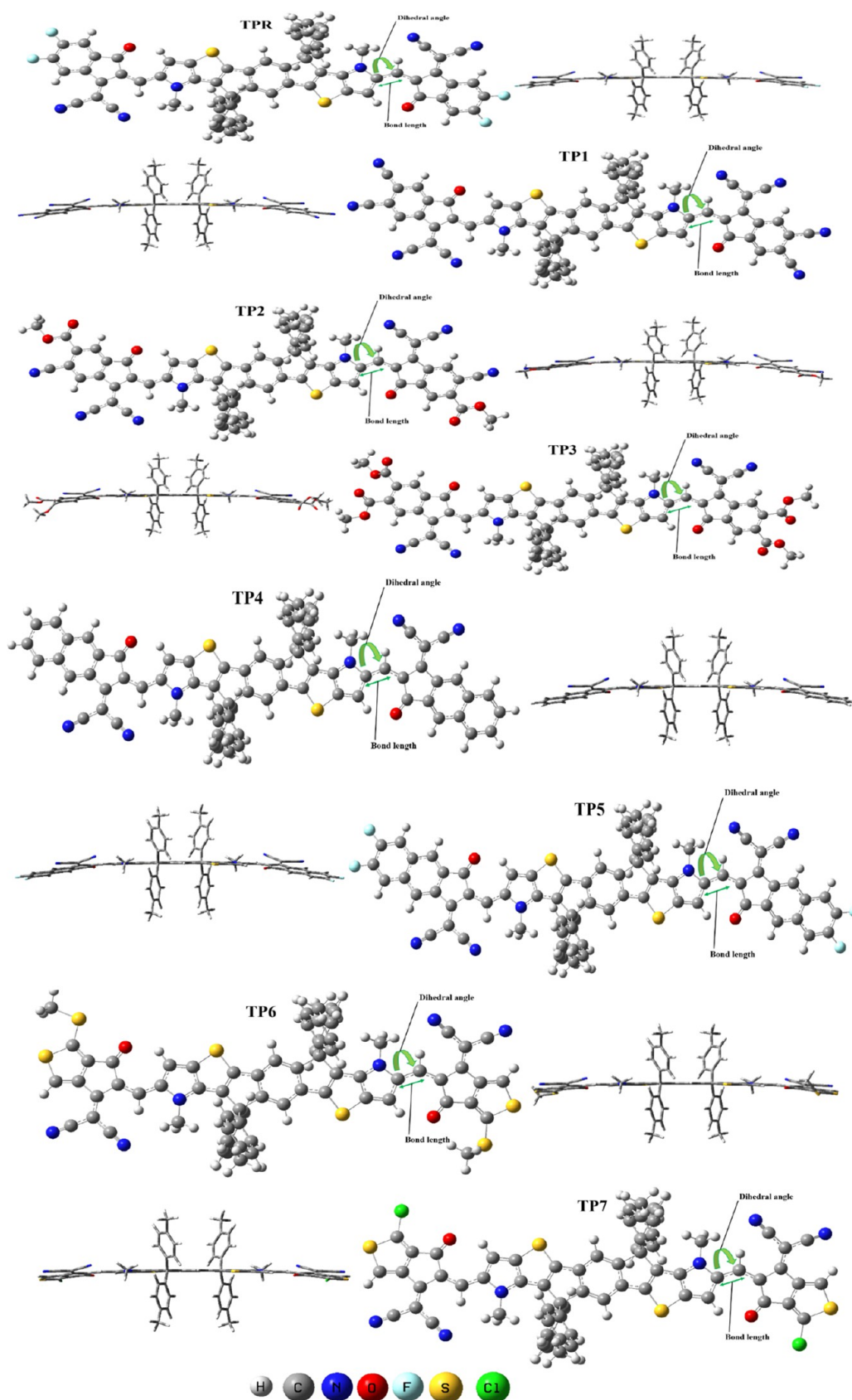


Figure 3. Top view of the ground state geometries in ball and bond type form, along with their lateral view in tube form.

were first globally optimized using the carefully selected B3LYP-D3 functional of the DFT level of theory at the 6-31G(d,p) basis set. These optimized geometries are revealed in

Figure 3, where the site of substitution between the donor and acceptor groups is indicated as well. It was seen that the new acceptor groups helped in retaining the overall planarity of the

molecules. The entire structure of the molecules was seen to be quite planar, except for the substituted four phenyl rings on the donor component of the molecules, which could help in conjugation and, thus, intramolecular charge transfer between two opposing regions of the molecule.³¹

The effect of substituted acceptors on their point of attachment was evaluated with the help of two easily understood bond parameters, i.e., the bond length and the dihedral angle.³² It is generally known that for the evaluation of the presence of effective conjugation at any bond, a strong indication is through the bond length.³³ If the bond length of a bond between two carbon atoms is in between the C–C bond length of 1.54 Å and the double one of 1.34 Å (C=C), then the bond is said to be conjugated. From the numerical values of bond lengths in Table 2, it is seen that all of the bond

Table 2. Evaluated Bond Parameters of the Molecules at the Substitution Site of the Acceptor Groups

molecules	dihedral angle (θ°)	bond length (Å)
TPR	1.69	1.41
TP1	1.84	1.40
TP2	1.62	1.40
TP3	1.25	1.41
TP4	1.77	1.41
TP5	1.47	1.41
TP6	1.04	1.41
TP7	1.11	1.41

lengths fall under the aforesaid range and, thus, are a clear indication of the conjugation within the molecules between the acceptor and donor components. Among all, the lowest bond length was measured for TP1 and TP2, making them better in terms of conjugation between the acceptor and donor components.

Another important parameter, which supports the overall conjugation and charge transmission within the molecular structure, is the dihedral angle.³⁴ The lower the dihedral angle at a specific site, the greater will be the planarity of the molecule at that point of substitution, and as a result, the higher would be the charge transfer in its structure. It was seen that though the reference molecule was quite planar with little-to-no torsion in-between both fragments (donor and acceptors), the designed molecules (except TP1 and TP4) seemed to have even greater planarity than the reference, as illustrated by their lower corresponding dihedral angles. Though the dihedral angles of TP1 and TP4 are slightly higher than that of the TPR molecule, they are not that much higher to be of much importance, and thus it could be said that all of the molecules, due to their planar configuration and conjugated bonds, between the donor and acceptor fragments could have an effective charge transfer within their structures, which might help in enhancing the overall photo-to-electric conversion efficiency (PCE) of the molecules.³⁵

3.3. Frontier Molecular Orbitals (FMOs). FMOs of the molecules at their ground state were studied to evaluate electronic density (wave function) at the corresponding HOMO and LUMO levels, together with their band gaps.³⁶ The electronic density distribution over the whole structure of the molecule determines the probability of electron transmission from the valence (HOMO) band toward the conduction (LUMO) band. Generally, if the HOMO electronic density is concentrated over the donor region of

the molecule, while the LUMO is more toward the acceptor components, then the effective transfer of an electron from the donor region toward the acceptor could take place within the molecule.³⁷ From Figure 4, it is seen that though the HOMO wave function of all of the molecules of this study follows the aforementioned trend, nevertheless, the LUMO wave function is distributed all over the molecule's plane, especially in TP6 and TP7. This spread of wave function over the entire structure might be ascribed to the planar geometry of the molecules, as both TP6 and TP7 have the lowest dihedral angles and thus the highest planarity, their wave function is the most dispersed one among all. Moreover, the nonexistence of any wave function over the perpendicular phenyl rings in the core of all of the researched molecules is accredited to their upright orientation concerning the rest of the plane of the structures.

Considering the FMOs in Table 3, the HOMO values follow the decreasing trend of TP4 > TP6 > TP5 > TP7 > TP3 > TPR > TP2 > TP1. On the other hand, this trend for LUMO energy levels is TP4 > TP6 > TP7 = TPR > TP5 > TP3 > TP2 > TP1. Therefore, the lowest lying HOMO and LUMO energy levels among all were seen to be of TP1, which points toward the probable proficient attributes of its corresponding acceptor fragments to stabilize the FMOs. On the contrary, the highest LUMO value of TP4 suggests its high open-circuit photovoltage if considered as an acceptor component in the photoactive layer of analogous OSC.³⁸

$$E_g = E_{\text{HOMO}} - E_{\text{LUMO}} \quad (2)$$

The above eq 2 was used to evaluate the band gap (E_g) between the FMOs (i.e., E_{HOMO} = HOMO's energy and E_{LUMO} = LUMO's energy). At this point, the lowest band gap of TP1 illustrates the enhanced electron-transferring characteristic of this molecule, which might be accredited to the high number of electron-withdrawing and highly unsaturated cyano groups present in its newly introduced acceptors. Correspondingly, the second-highest number of unsaturated cyano groups in TP2 could have made its band gap the second lowest among all.

Overall, the declining order of band gaps among all of the investigated molecules, TPR > TP3 = TP6 > TP4 = TP7 > TP5 > TP2 > TP1, shows that all of the proposed molecules have improved charge-transfer aptitude compared to the reference due to their comparatively lower band gaps. Between TPR and TP5, the only difference is the additional phenyl ring in the case of the latter. By enhancing the conjugation within the molecule, this phenyl ring lowered the band gap in the corresponding TP5 molecule as compared to TPR. Therefore, all of the molecules, though minutely, could be better for the photoactive layer than the reference with regard to their band gaps.

3.4. Density of States. In a pursuit to solidify the findings of FMO examination, the density of states of all of the molecules of this study was computed at the selected functional and D3 dispersion parameters of DFT. These density of states (DOS) are quite helpful in determining the probability of any electron residence within a specific energy state (either FMOs or any other) and helps in evaluating the participation of any component of a molecule (donor or acceptor) in developing the FMOs.²⁹ In the graphs of DOS, the vertical axis depicts the relative intensities of the energy levels, while the lower horizontal axis portrays the energy in electron volts (eV).

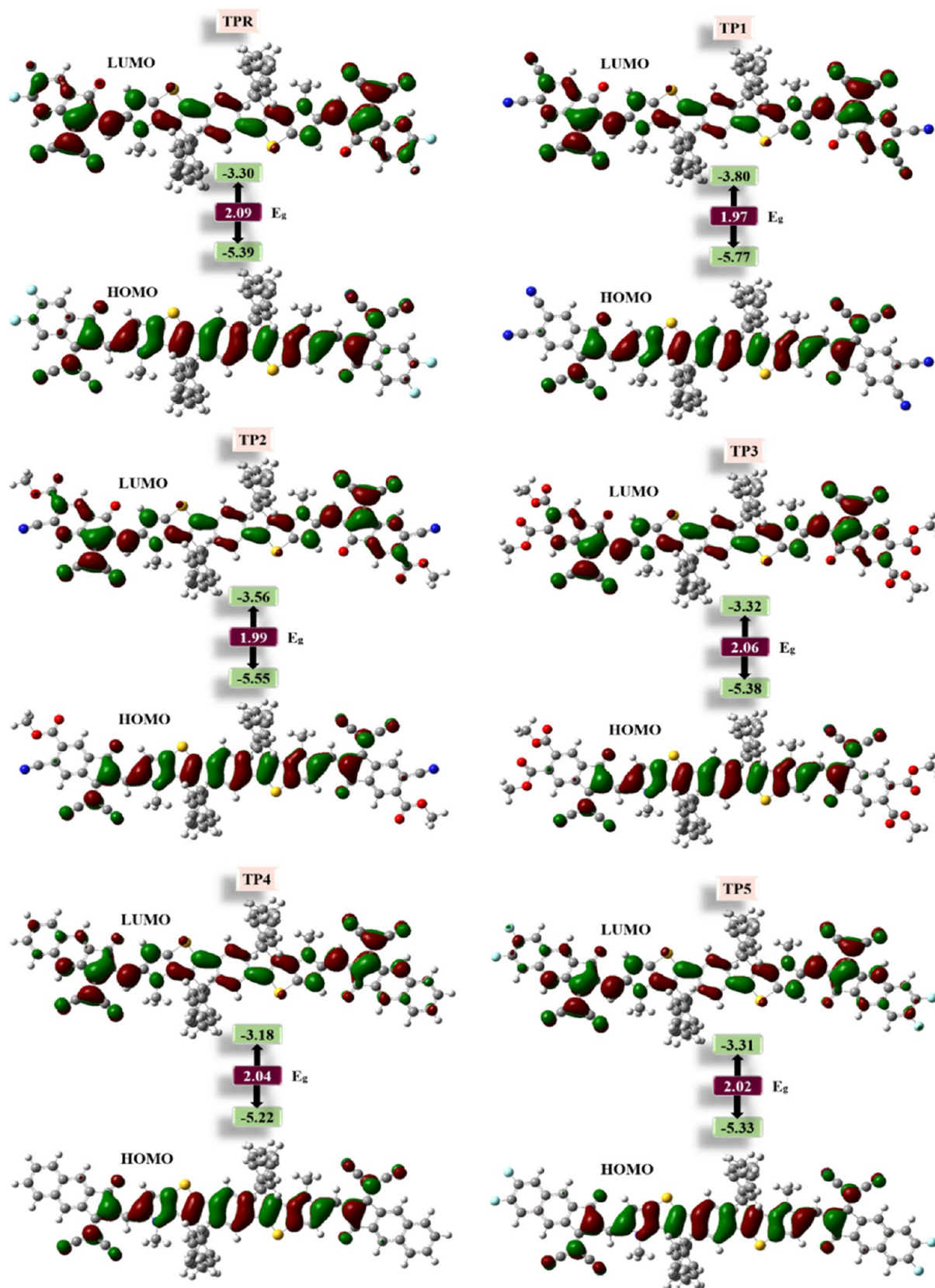


Figure 4. continued

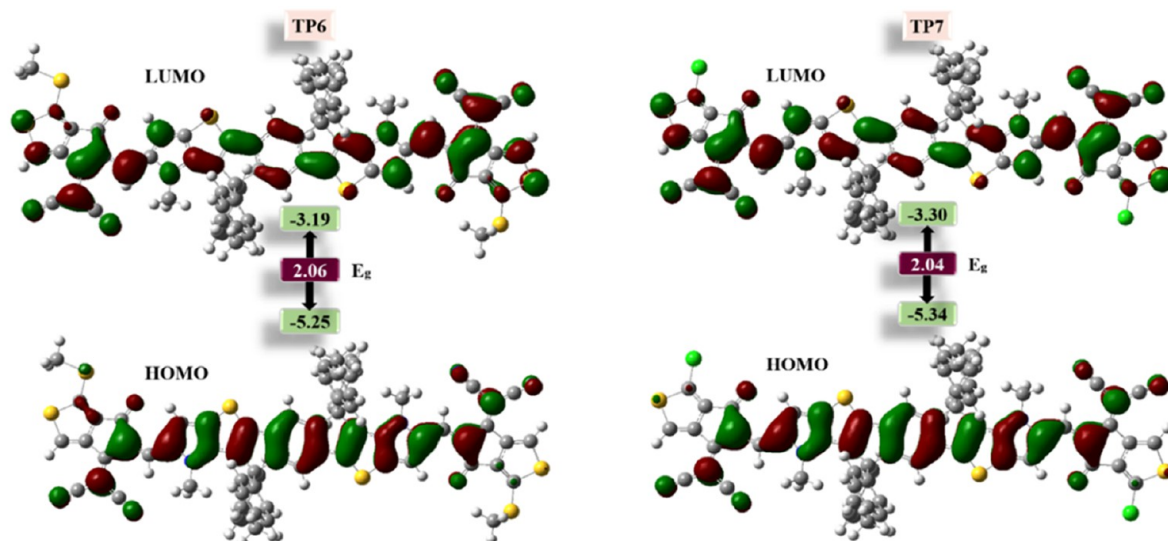


Figure 4. Pictorial representation of the charge density dispersal, along with the values of the studied FMOs and associated band gaps of the researched molecules.

Table 3. Studied FMOs of All of the Molecules under Study, Along with Their Computed Band Gaps (E_g)

molecules	E_{HOMO} (eV)	E_{LUMO} (eV)	E_g
TPR	-5.39	-3.30	2.09
TP1	-5.77	-3.80	1.97
TP2	-5.55	-3.56	1.99
TP3	-5.38	-3.32	2.06
TP4	-5.22	-3.18	2.04
TP5	-5.33	-3.31	2.02
TP6	-5.25	-3.19	2.06
TP7	-5.34	-3.30	2.04

For the generation of curve plots of DOS, the structures of the molecules were fragmented into separated donor and acceptor components; this way, the contribution of both of them in the total DOS was easy to assess. As a result, in Figure 5, the sharp black peaks portray the total DOS of the overall molecule, while the blue and red ones depict the partial DOS of the donor core and the acceptor fragments, respectively. Here, in relation to the FMOs, the sharp peaks with negative energy values near -5.0 eV represent the HOMO energy state, whereas the ones just toward the right of the central planar band gap region illustrate the LUMO energy levels. Additionally, this planar region in the middle of the DOS curve plots was actually seen to be in correspondence with the band gap of the FMOs.

In addition to the plots of DOS, the numerically compiled percentages of the participation of both fragments in developing the molecules' FMOs are shown in Table 4. Even here, the percentage involvement of each region in raising either the HOMO or the LUMO matches well with the charge dispersal in the FMO analysis. Thus, the effective charge dispersal abilities of the molecules could be seen by the greater contribution of the donor core toward HOMO and vice versa. Between TP1 and TP3, the difference is only in the number of highly unsaturated cyano or acetyl groups at the peripheries of the molecules. Here, it can be seen that the percentage contribution of the LUMO energy level in all three molecules is directly associated with the greater number of the CN groups, which is why TP1, with its highest number of cyano

groups, has the highest LUMO percentage of the acceptor groups. Moreover, despite the rather similar acceptor groups in both TP4 and TP5, the presence of a greatly electron-withdrawing fluoro group at the margins of TP5 has slightly enhanced the acceptor contribution in LUMO development. Likewise, the chloro group in the acceptor of TP7 has increased its acceptor's LUMO percentage as opposed to the TP6 molecule.

3.5. Characterization of Optical Attributes. The efficient excited state properties of the organic chromophores are quite essential in amplifying the light harvesting and absorption properties of the corresponding organic photovoltaic cells (PVs).³⁹ In this aspect, the excited state features of all of the modeled molecules and TPR were computed in both the gaseous state and the chloroform (CF) medium. In Tables 5 and 6, the absorption maxima (λ_{max}), first excitation energies, dipole moment, and interaction coefficient of all of the studied molecules taken using the B3LYP/D3/6-31G(d,p) level of theory are compiled for CF and gaseous medium, respectively. This dispersion parameter with the B3LYP functional is known to give the most accurate absorption and electronic results relative to the experimental data.⁴⁰ The absorption spectra of all of the molecules in both the analyzed mediums are presented in Figure 6.

A bathochromic shift in the absorption maxima of the newly proposed molecules could be perceived in both the analyzed mediums. In gaseous and CF mediums, the λ_{max} follows the declining order of TP1 > TP2 > TP5 > TP4 > TP3 > TP7 > TP6 > TPR and TP1 > TP2 > TP5 > TP3 > TP4 > TP7 > TP6 > TPR, respectively. Between these two orders, the highest λ_{max} is observed to be of TP1 and TP2 molecules, both of which till now seems to be quite proficient due to their lowest band gap and now the highest λ_{max} with a red shift of 55 and 40 nm in solvent medium and 41 and 30 nm in the gas phase for TPR. Due to the slightly similar structural morphology of TP2 with TP1 molecule (having the difference of only the acetyl group in TP2 compared to the cyano of TP1), their higher λ_{max} could be ascribed to the greater electron-withdrawing power, in addition to the high unsaturation of cyano groups. Similarly, the greater electron-withdrawing capability of the fluoro group of acceptors of TP5

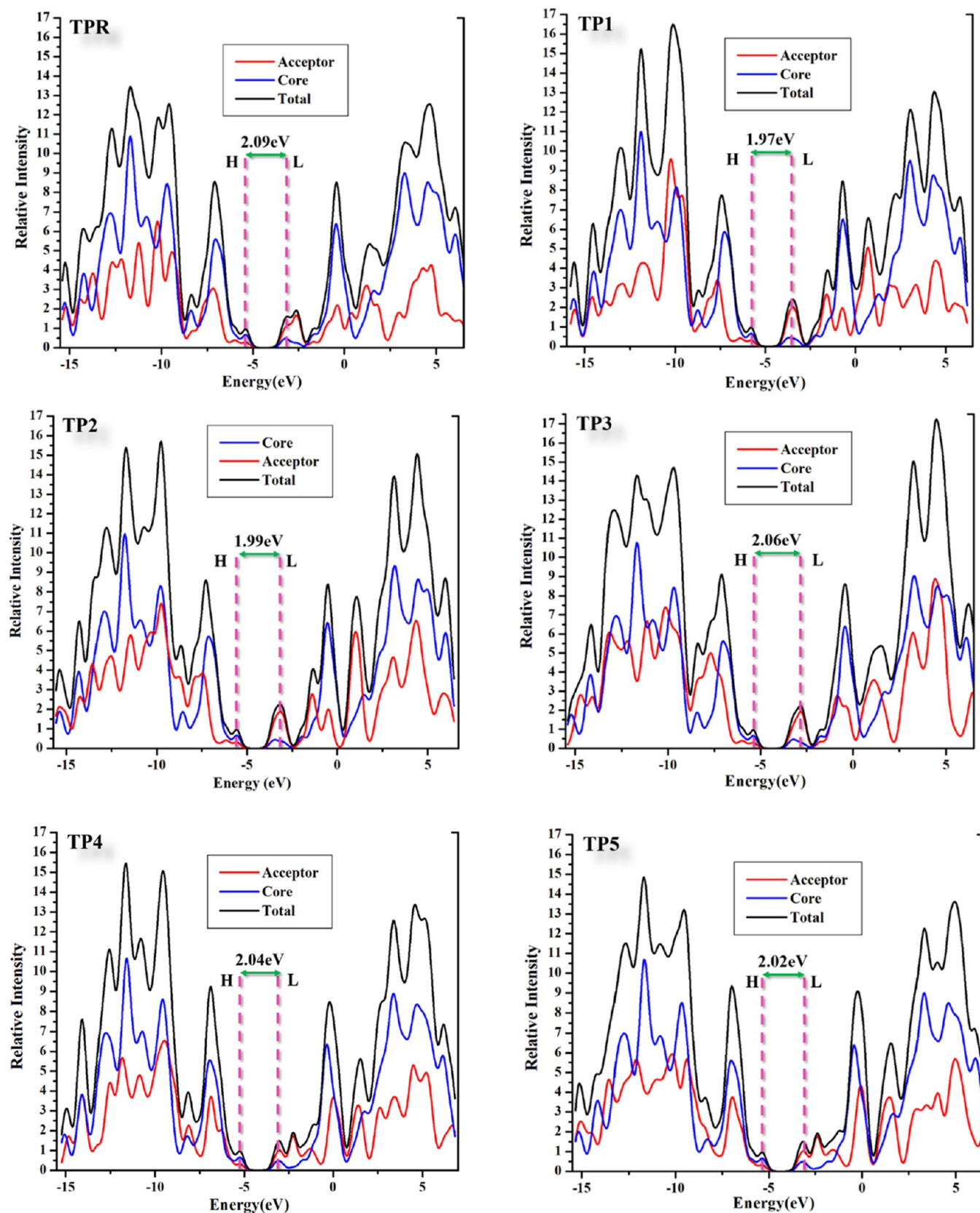


Figure 5. continued

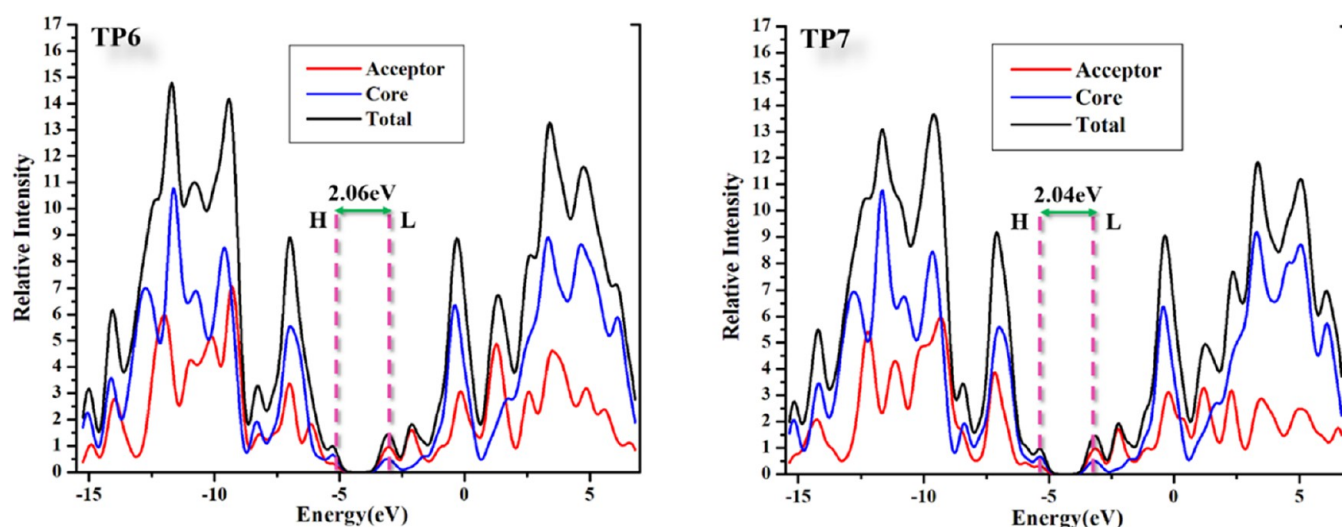


Figure 5. Total and partial DOS of the fragments (acceptor and core) of the molecules.

Table 4. Contribution of Both Donors and Acceptors in Developing the FMOS's Wave Functions

molecules	FMOs	acceptor (%)	core (%)
TPR	HOMO	29.9	70.1
	LUMO	63.6	36.4
TP1	HOMO	31.6	68.4
	LUMO	68.5	31.5
TP2	HOMO	31.3	68.7
	LUMO	67.8	32.2
TP3	HOMO	30.5	69.5
	LUMO	64.0	36.0
TP4	HOMO	31.7	68.3
	LUMO	63.7	36.3
TP5	HOMO	31.8	68.2
	LUMO	64.1	35.9
TP6	HOMO	32.2	67.8
	LUMO	62.1	37.9
TP7	HOMO	31.3	68.7
	LUMO	63.0	37.0

Table 5. Computed λ_{\max} , E_x , Dipole Moments, and Interaction Coefficient of All Molecules in the Gas Phase at the TD-DFT/B3LYP/D3/6-31G (d,p) Level of Theory

molecules	computed λ_{\max} (nm)	E_x (eV)	μ_{gas} (Debye)	interaction coefficient
TPR	658.69	1.8823	0.552500	0.70387
TP1	698.03	1.7762	1.858500	0.70118
TP2	688.44	1.8009	0.148201	0.70256
TP3	667.78	1.8567	0.937238	0.70358
TP4	672.51	1.8436	2.075200	0.70482
TP5	678.17	1.8282	0.907400	0.70492
TP6	665.78	1.8622	3.359086	0.70528
TP7	666.23	1.8610	0.238700	0.70607

could also be the reason behind its higher λ_{\max} . The numerical values of absorption maxima in both mediums imply the greater proficiency of the chromophores in the selected solvent than in the gas phase. On a side note, from the absorption spectra in Figure 6, it can be seen that TP4–TP7 molecules have additional minor peaks near 400 nm, besides the intramolecular charge transfer (ICT) ones near 700 nm.

These peaks illustrate the better π – π^* stacking in these molecules as opposed to the other proposed molecules of this study.⁴¹

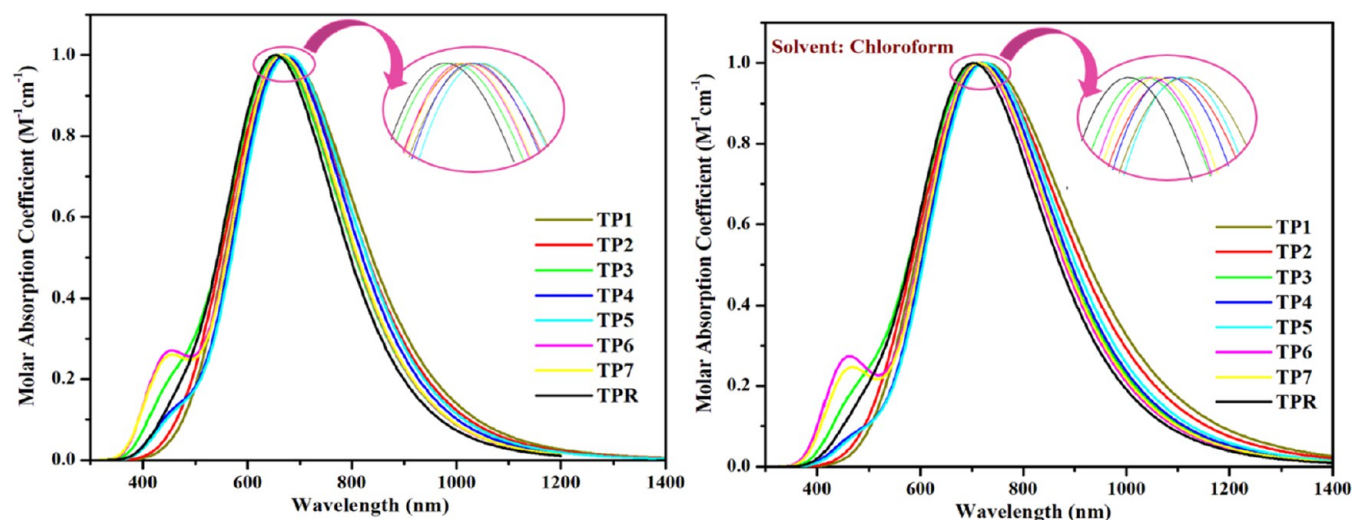
The first excitation energy is the amount of energy that could be needed by a molecule for the transmission of an electron from the valence/HOMO band to the conductance/LUMO band.⁴² A general trend for this energy is that it should be lowered for effective electron transfer between states.⁴³ Subsequently, as all of these reported molecules have lower excitation energies than TPR, they should have better electron transfer between their FMOs than the reference. Individually, the lowest excitation energies among all appear to be of TP1 and TP2 molecules, with TP1 being the lowest one in both the studied phases. So far, it seemed that though all of the proposed molecules could act as better contenders than TPR, TP1 and TP2 might be the best ones of all.

Additionally, the dipole moments of all of the molecules in both the phases being studied contributed significantly to supporting our claim that the newly reported molecules are more effective than TPR. The dipole moment is quite imperative in determining the stability of the molecules in the given medium, and its higher numerical value promotes crystallinity and charge carriers' mobility between the molecules at the interface between the donor and acceptor components at the photoactive layer of solar cells. The high value of dipole moment can also lead to a reduced number of disorder-influenced trap states, which in turn could enhance the fill factor of the molecule.⁴⁴ Generally, a greater value of dipole moment in the solvent phase than in the gas phase justifies the utilization of the considered chromophores through solution-processable techniques of OPV construction, which makes our proposed chromophores quite sustainable in the chosen chloroform solvent.⁴⁵ Furthermore, the highest dipole moments of TP6 could be chalked up to be due to the two-five-membered ring framework (cyclopenta[*c*]thiophene) of its terminal acceptor moieties having perpendicular –SCH₃ groups. The lower dipole moment of TP7, despite its similar structure to TP6, could be due to its lowest dihedral angle and highly planar structure throughout the acceptor rings.

Moving on, the last studied absorptive parameter for the analyzed chromophores was the interaction coefficient, which is generally believed to be the lower the better in the case of

Table 6. Computed and Experimental λ_{\max} , E_x , Dipole Moments and Interaction Coefficient of All Molecules in Chloroform Medium

molecules	computed λ_{\max} (nm)	experimental λ_{\max} (nm)	E_x (eV)	μ_{solvent} (Debye)	interaction coefficient
TPR	708.25	732	1.7506	0.750900	0.70200
TP1	763.36		1.6242	2.176700	0.70153
TP2	747.73		1.6581	0.120701	0.70181
TP3	722.25		1.7166	1.035544	0.70193
TP4	720.84		1.7200	2.572400	0.70197
TP5	726.70		1.7061	1.209300	0.70215
TP6	713.06		1.7388	3.862788	0.70246
TP7	715.40		1.7331	0.332300	0.70321

**Figure 6.** Absorption graphs of all eight molecules (TPR, TP1–TP7) in both the mediums under study.

organic solar cells. This interaction coefficient, just like oscillating strength, is a dimensionless parameter and illustrates the degree of interaction between generated excitons (electron–hole pair) in the chromophores.⁴⁶ And for the excitons to conveniently move toward their respective electrodes, the interaction between them needs to be lowered, which is the case in the TP1–TP4 molecules in both phases of study. So, despite having a rather low dipole moment, TP2 sounds to be better than the reference.

Taking into account the absorption profile of the scrutinized molecules, it could be concluded that all our newly reported molecules could act as superior chromophores in the photoactive layer of OPVs compared to the reference in one way or another.

3.6. Exciton Dissociation Energy. A decisive parameter for the determination of the effectiveness of the studied chromophores is their exciton dissociation energy, generally acknowledged as the binding energy. It is essentially the amount of energy needed when the generated electron and hole pair, i.e., the excitons, have to disintegrate and move toward their corresponding electrodes.⁴⁷ With low numerical values of this energy, the phenomenon of recombination between the excitons can be diminished significantly, which is one of the leading causes of lowered PCE of OPVs. The exciton dissociation or binding energy of all of the researched molecules was calculated with eq 3.⁴⁸

$$\text{EDE} = E_g - E_x \quad (3)$$

Here, EDE is the exciton dissociation/disintegration energy, E_g is the band gap between the FMOs, and E_x is the computed 1st

excitation energy of the molecules. EDE was computed by taking into use the band gap values from Table 2 and the E_x values from Tables 5 and 6 for both the CF and gas phases, respectively. The values of EDE in Table 7 suggest that all of

Table 7. Exciton Dissociation Energies (EDE) of All of the Molecules in Both the Analyzed Mediums

molecule	EDE gas (eV)	EDE solvent (eV)
TPR	0.207	0.339
TP1	0.194	0.341
TP2	0.189	0.332
TP3	0.203	0.343
TP4	0.196	0.320
TP5	0.192	0.314
TP6	0.198	0.321
TP7	0.179	0.307

the newly suggested molecules have better chances of charge carriers' movement within their structure than the reference TPR. Also, in the gas medium, the lowest EDE value of TP7 implies its better capabilities among all, with TP2 being a close second. But in the chloroform medium, though TP7 still has the lowest EDE value, TP5 now seems to have the next lowest EDE value. This seemingly different trend in chloroform (CF) compared to the gas phase implies the enhanced attributes of some of our proposed compounds in the CF medium.⁴⁹ In addition, between the two studied phases, the higher values of EDE in the CF (chloroform) phase than in the gas phase actually signify the greater interactions between the respective

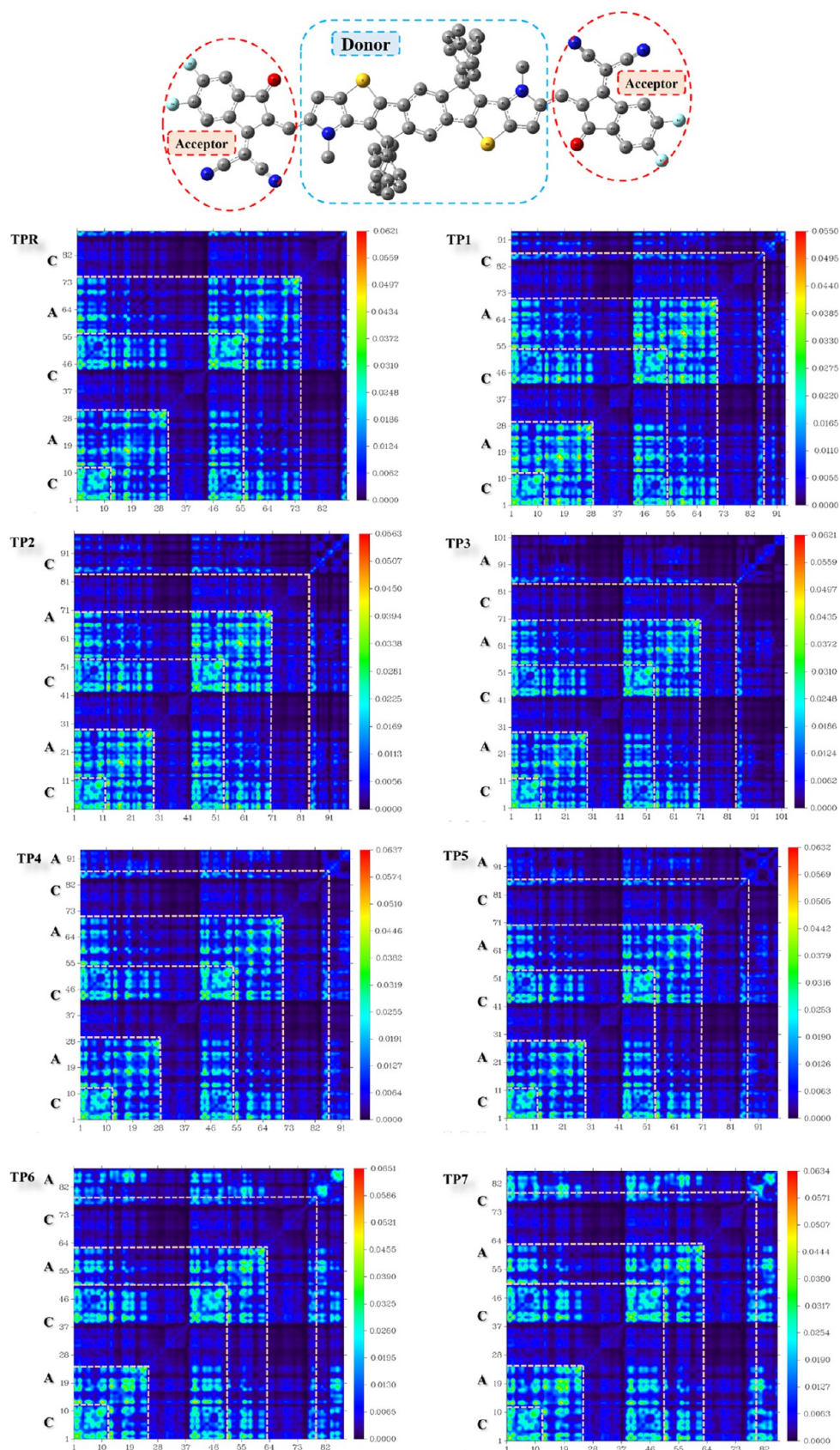


Figure 7. Generated TDM maps of all of the scrutinized molecules (TPR, TP1–TP7).

chromophore and the solvent of study.⁴⁵ Besides, in the CF phase, except for TP1 and TP3, all of the molecules proposed here have lower EDE than the reference molecule; even then,

the EDE of TP3 is quite comparable to the reference molecule. Therefore, it seems that almost all of the proposed chromophores might perform better in terms of their excited

state attributes than the reference at the photoactive layer of OPV cells.

3.7. Transition Density Matrix. TDM analysis is known to be an effective approach to examine the electronic dispersion, as well as charge separation and transition sites after photon absorption in the molecule under consideration.⁵⁰ It also demonstrates the quantum geometric features and the electronic transition between the acceptor and donor parts of the molecules.⁵¹ The TDM study of all of the examined molecules was performed at the selected level of TD-DFT-D3, and 3D colored visualizations of the obtained results were created using the Multiwfn 3.7 application.

It is generally seen that all of the molecular atoms participate in the electronic transition, except for hydrogens. This is the reason behind their exclusion in this analysis of the TDMs of the researched molecules.⁵² The thus generated TDM plots were segmented into two portions: the donor core (C) and end-capped acceptor moieties (A), according to the number of atoms present along their lower *x* and left *y*-axes (Figure 7). Also, in the colorful plots of TDM, the vertical axis on the right portrays the colored bar demonstrating the electronic density present along the structure of the respective molecule. Here, the blue and red colors symbolize the lower (zero) and highest charge density levels, respectively, while the yellow, cyan, and green colors indicate the densities of intermediate transitions. Consequently, in the actual 2D maps, the brightly colored patches reflect the significant contribution of atoms in electronic excitation and the availability of transition sites within the molecules, and blue ones depict the contrary.⁵³ Precisely, in all of the cores of the plots, it can be perceived that the number of atoms illustrating the perpendicular phenyl rings has zero charge density (dark blue hued), while the ones depicting the remaining atoms of the core have high charge density, both diagonally and off-diagonally. This presence of charge density in the core of the molecules illustrates the electron richness of their donor regions. On the other hand, only TP6 and TP7 show high charge density even at the terminal ends of their acceptor regions, which portrays better charge dispersal over the whole plane of both these molecules. This distribution of charge density could be ascribed to the high planarity between the cores and highly electron-withdrawing acceptors of these molecules.

3.8. Chemical Reactivity Indices. To approximate the better charge-transfer attributes of the suggested chromophores in comparison to the reference TPR, their reactivity indices, including ionization potential (IP), electron affinity (EA), chemical hardness (*H*), and softness (*S*), were calculated with the help of eqs 4–7.^{31,33}

$$IP = [E_0^+ - E_0] \quad (4)$$

$$EA = [E_0 - E_0^-] \quad (5)$$

where E_0^+ and E_0^- are the energies of cation and anion of their ground state optimized geometries, respectively. While E_0 illustrates the neutral molecule's energy at its ground state.

$$H = \frac{(IP - EA)}{2} \quad (6)$$

$$S = \frac{1}{2H} \quad (7)$$

From the above equations, it is distinctly clear that softness (*S*) is actually reciprocal to twice the hardness (*H*), which is half of

the difference between ionization potential and electron affinity.⁵⁴

Generally, a low value of ionization potential is related to the high HOMO value and the easier electron-donating properties of the molecule, while a high electron affinity is associated with a high LUMO energy level and relatively high electron-accepting attributes of the molecule.⁵⁵ In addition, molecules with high EA and low IP values tend to have a greater reactive nature than those having low EA values. All of the newly developed molecules of this study, except TP1 and TP2, had lower IP than TPR, which depicts their higher reactivity, but the rather higher IP of TP1 and TP2 could be said to be due to their more stabilized HOMO energy values. Similarly, the higher EA of all of the reported molecules, except TP4 and TP6 (due to their low-lying LUMO state), portrays their higher electron-accepting abilities than TPR. Taking these values into account, it was assumed that our proposed molecules might perform as superior acceptors.

Continuing toward chemical hardness and softness, molecules having low chemical hardness and high softness values illustrate better reactivity than vice versa. And from Table 8, it is perceived that all of the newly suggested

Table 8. Computed Chemical Reactivity Indices of All Investigated Molecules in eV

molecules	IP	EA	η	S
TPR	6.169	2.536	1.816	0.275
TP1	6.535	3.065	1.735	0.288
TP2	6.317	2.821	1.748	0.286
TP3	6.147	2.582	1.782	0.281
TP4	5.975	2.456	1.759	0.284
TP5	6.084	2.586	1.749	0.285
TP6	6.016	2.446	1.785	0.280
TP7	6.122	2.546	1.788	0.279

molecules have a higher softness and lower hardness than the reference TPR. The softness values of the molecules of this research work follow the escalating order of TPR < TP7 < TP6 < TP3 < TP4 < TP5 < TP2 < TP1, and being reciprocal to it, hardness has the reverse order to the aforementioned one. Therefore, while TP1, with its higher EA and *S*, as well as the lowest *H* value, is discerned to have the highest reactivity, all of the suggested molecules have superior attributes compared to the reference. Specifically, TP4–TP7 molecules, in addition to having higher EA and *S*, and lower *H* than TPR, have lower IP values as well. Consequently, these four molecules might be proficient acceptors in the blend of organic materials in the photoactive layer.

3.9. Molecular Electrostatic Potential (MESP) Surfaces. The study of (MESP) surfaces is very crucial for comprehending the distribution of electrostatic potential on various parts of a molecule. This parameter highlights the different parts according to their susceptibility to electrophilic or nucleophilic attack.⁵⁶ A color scheme is used to show the extent of electrostatic potential, with red contours at one extreme, for areas where the negative potential is significantly high, while the blue ones, at the other extreme, represent very low electron potential. Cyan-contoured areas are also associated with relatively low electron potential but slightly higher than dark blue color zones. The contrary is the case for orange and yellow regions. Finally, the green color points toward those parts that have intermediate electron potential, in

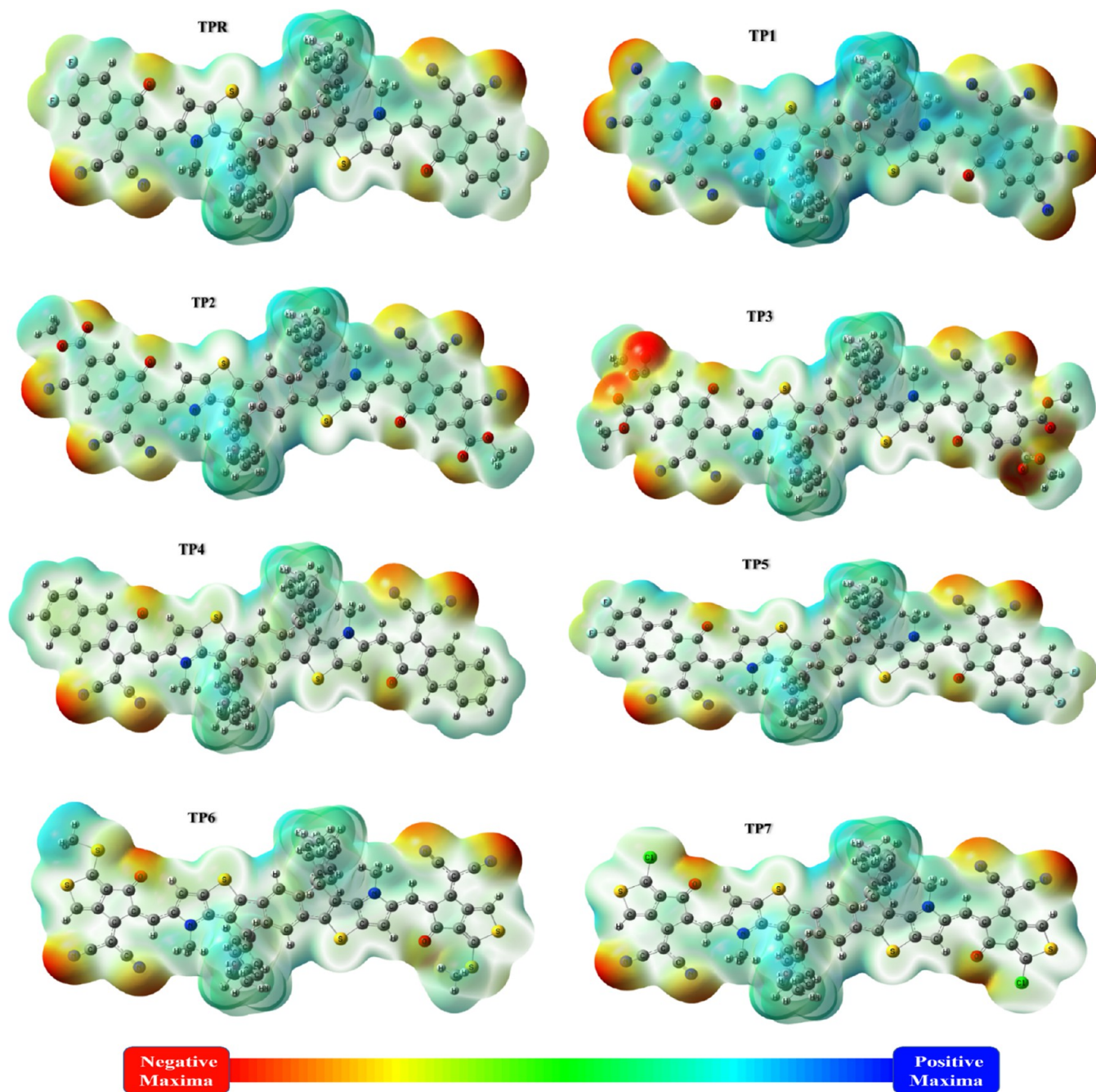


Figure 8. Formulated MEP surfaces of all of the molecules at their ground state.

other words, neutral zones. Precisely, a nucleophilic attack can occur in blue zones, while red color parts are more exposed to electrophilic attack.⁵⁷

It is observable from Figure 8 that negative potential sites are essentially present on the acceptors of the studied molecules because of the more electronegative, as well as unsaturated nitrogen and oxygen atoms present there, which pulls the electron density toward themselves and increases their electrostatic potential. Though the fluorine and chlorine of TP5 and TP7, respectively, are quite electron-withdrawing moieties, the absence of unsaturation in their bonds has slightly lowered their electron potential in comparison to the unsaturated nitrogen and oxygen atoms. On the other side of the spectrum, the nitrogen of the cores of the molecules is surrounded by cyan or blue colors, which could be ascribed to

the absence of unsaturation in its bond. Actually, the cores of all of the structures are of cyan and greenish color, emphasizing their lower electron potentials. Furthermore, these distinct colored areas demonstrate a great extent of charge separation in these structures, which could promote effective charge dispersal between the central donor and the peripheral acceptors. In the case of the proposed molecules, the better separation of electron potential in them as compared to TPR indicates excellent charge-withdrawing properties of these newly introduced acceptors. Individually, the darkest blue shade could be seen in the TP1 molecule, which shows the highest electron-withdrawing attributes of its cyano groups, but this enhanced blue zone might lower its chances as an efficient acceptor in the photoactive layer because it is seen to be spread over the whole molecule, whether acceptor or donor, which

Table 9. Reorganization Energies, Charge-Transfer Integral, and Rate Constant of Charge Hopping of Both the Excitons (Hole and Electron) of All of the Molecules

molecule	$\lambda_{\text{electron}}$ (eV)	t_{electron} (eV)	k_{electron} (s ⁻¹)	t_{hole} (eV)	λ_{hole} (eV)	k_{hole} (s ⁻¹)
TPR	0.146814	0.134832	8.33×10^{14}	0.298373	0.198134	7.2×10^{16}
TP1	0.100277	0.099458	1.87×10^{15}	0.294427	0.189636	1.23×10^{15}
TP2	0.118438	0.106260	1.20×10^{15}	0.293067	0.196270	2.50×10^{16}
TP3	0.147573	0.128846	7.44×10^{14}	0.294835	0.205206	3.23×10^{16}
TP4	0.127780	0.144764	1.75×10^{15}	0.281910	0.184988	1.23×10^{15}
TP5	0.128147	0.143268	1.70×10^{15}	0.284495	0.190204	1.13×10^{15}
TP6	0.143635	0.155377	1.26×10^{15}	0.271025	0.183144	1.20×10^{15}
TP7	0.137684	0.150071	1.41×10^{15}	0.289121	0.189100	1.16×10^{15}

could reduce the overall charge separation and electron-withdrawing abilities of the molecule.

3.10. Charge-Transfer Rate. For the assessment of the charge mobility rate of the charge carriers in the molecules, the rate constant for charge hopping was determined according to eq 1 from Marcus theory. According to this theory, the charge carriers remain within the molecule, while the charge hops between adjacent molecules, and it is believed that the greater the rate constant for charge hopping, the better would be the charge mobilities in the molecule.^{44b} The above-mentioned equation shows that the charge integral (t_{electron} and t_{hole}) has a direct association with the rate constant, while reorganization energy ($\lambda_{\text{electron}}$ and λ_{hole}) has an inverse one. The values of both these parameters were calculated according to the equations below and were utilized to compute the rate constant (k) for all of the molecules of this study.

First, the reorganization energy is generally known as the energy required by the molecule to reorganize the changes in its geometry after the transfer of holes and electrons in its structure. The numerical values of reorganization energies of holes and electrons could be determined by eqs 8 and 9.⁵⁸

$$\lambda_{\text{electron}} = [E_{-}^0 - E_0] + [E_0^{-} - E_{-}] \quad (8)$$

$$\lambda_{\text{hole}} = [E_{+}^0 - E_0] + [E_0^{+} - E_{+}] \quad (9)$$

In the above equations, E_0^{-} and E_0^{+} are the ground state anionic and cationic energies of neutral molecules, respectively. E_{-}^0 and E_{+}^0 are the neutral energies of the optimized anion and cation of the molecules. While E_{-} and E_{+} are optimized anionic and cationic energies, respectively. Finally, E_0 is the energy of the neutral molecule at its ground state.⁵⁹

From Table 8, it is identified that all of the newly described molecules (except the comparable one of TP3) have, in comparison to the reference, lower electron and hole reorganization energies. This illustrates their more enhanced aptitude as either donor or acceptor material in the blend of organic materials in the photoactive layer than TPR. Exclusively, between $\lambda_{\text{electron}}$ and λ_{hole} , the relatively lower electron reorganization energy values of all of the molecules of study support our statement of the newly proposed molecules being proficient acceptors.

The second important factor directly related to the rate constant, i.e., the charge integral of electron and hole, was also calculated with the assistance of eqs 10 and 11.¹⁹

$$t_{\text{electron}} = \frac{E_{L+1} - E_L}{2} \quad (10)$$

$$t_{\text{hole}} = \frac{E_H - E_{H-1}}{2} \quad (11)$$

where the energies of LUMO + 1 and HOMO - 1 are represented by E_{L+1} and E_{H-1} , respectively, while E_H and E_L are the energies of HOMO and LUMO, respectively. On the contrary to the reorganization energy, the higher the value of the charge integral of a molecule, the higher will be its rate constant of charge hopping. The values of charge integral imply that in the case of t_{hole} , all of the newly proposed molecules have seemingly lower numerical values than the reference. But in the case of t_{electron} , the numerical values of TP4–TP7 were seen to be higher than that of the TPR molecule. Actually, with the lowest $\lambda_{\text{electron}}$ of TP1, its lowest t_{electron} seemed to be redundant. But overall, it could be said that both the reorganization energy and charge integral for electrons of TP4–TP7 were seen to be better than the reference molecule, making them quite effective acceptor molecules.

From the values of the above-computed parameters, the values for the rate constant of electron (k_{electron}) and hole (k_{hole}) hopping were evaluated and are organized in Table 9. It is understood that the k_{hole} of all of the newly proposed molecules is lower than the reference molecule; on the contrary, the k_{electron} of all, except TP3, seems to be higher than the reference TPR molecule. Therefore, it was evaluated that our newly reported molecules, excluding TP3, might act as better acceptors than the reference molecule. The low electron mobility properties of TP3 could be accredited to the less electron-withdrawing acetyl groups present at the terminal ends of its acceptors.

3.11. Light-Harvesting Efficiency. Among the researched acceptors in Table 10, the highest oscillating strength (f), which is an important parameter related directly to the light-harvesting efficiency (η_i), was seen to be of the TP4 molecule (with TP5 being a close second) in both the evaluated mediums. Moreover, the oscillating strength of all of the newly proposed molecules, except for TP1 and TP2, was perceived to

Table 10. Computed Light-Harvesting Efficiencies and Oscillator Strength of the Molecules in the Solvent and Gas Phases

molecules	f_{os} (solvent)	η_{solvent}	f_{os} (gas)	η_{gas}
TPR	2.6703	0.9980	2.4208	0.9962
TP1	2.1598	0.9931	2.1334	0.9926
TP2	2.3653	0.9960	2.2556	0.9944
TP3	2.6871	0.9980	2.5552	0.9972
TP4	3.1269	0.9993	2.8518	0.9986
TP5	3.1147	0.9993	2.8464	0.9986
TP6	2.9120	0.9988	2.6034	0.9975
TP7	2.9252	0.9988	2.6176	0.9976

be higher than the reference molecule, which indicates their better light-harvesting efficiency as well.^{44b}

$$\eta_{\lambda} = 1 - 10^{-f} \quad (12)$$

η_{λ} in eq 12 is known to be an important scale for the determination of the amount of light utilized in excitons generation after its absorption by the chromophore and has quite a significance in evaluating the photo-to-electric conversion efficiency (PCE) of any chromophores as it has a direct association to the short-circuit current density, which is directly linked to the PCE, eqs 13 and 14.⁶⁰

$$J_{SC} = \int_{\lambda}^0 \eta_{\lambda}(\lambda) \phi_{\text{injected}} \eta_{\text{collect}} d\lambda \quad (13)$$

Here, the efficiency of electron injection is ϕ_{injected} , and that of charge-collection is η_{collect} .⁶¹

$$\text{PCE} = \frac{J_{SC} V_{OC} \text{FF}}{P_{in}} \quad (14)$$

P_{in} is the incident radiations' power, J_{SC} is the short-circuit current density, V_{OC} is the open-circuit photovoltage, and FF is the fill factor.⁶² The latter two factors are computed for the molecules of this study in the latter section as well.

Comparatively, the identical η_{λ} of TP6 and TP7 (as well as TP4 and TP5) in both the mediums could simply be ascribed to the similar ring skeleton of their acceptor groups. On the contrary, the rather low values of η_{λ} in TP1 and TP2 could be said to be due to the high cyano groups in their similar acceptor ring skeletons, which, while enhancing the optoelectronic attributes of the molecules, might have lowered their oscillating power and, by association, the light-harvesting efficiency.

3.12. Photovoltaic Attributes as Acceptors. At last, two imperative photovoltaic parameters, which according to eq 14 are directly related to the photo-to-electric conversion efficiency of any chromophore, were calculated through eqs 15 and 16. These are the open-circuit photovoltage (V_{OC}) and the fill factor (FF). Between these two, V_{OC} is of quite significance because of the fact that the theoretical evaluation of the FF is also made possible with the help of V_{OC} .

Open-circuit photovoltage is essentially the voltage produced by the chromophore when there is little-to-no externally supplied current. It greatly depends on the temperature, intensity of light, and, most importantly, the FMOs of the donor and acceptor materials at the interface. Basically, for the determination of the V_{OC} , the FMOs of both the donor and acceptor are aligned adequately, and with the help of eq 15,⁶³ its numerical value is determined.

$$V_{OC} = \frac{1}{e} (E_{\text{LUMO of acceptor}} - E_{\text{HOMO of donor}}) - 0.3 \quad (15)$$

In this equation, $e = 1$ and is the charge on the molecules, while 0.3 is the empirical value employed to eliminate any probable overestimation in the theoretical determination of V_{OC} . Furthermore, the terms in parenthesis depict the difference in-between LUMO's value of the acceptor molecule and HOMO's value of the donor. Therefore, this equation portrays the relation between the FMOs of the considered molecules in the photoactive layer.⁶⁴ Here, as all studied molecules were taken as acceptors, a commonly known and prominent donor for theoretical computations, i.e., PTB7-Th, was utilized in association with them. The hence calculated

V_{OC} values are compiled in Table 11 and pictorially illustrated in Figure 9 as well.

Table 11. Calculated Photovoltaic Parameters of All of the Molecules under Investigation

molecule	V_{OC} (V)	E_{loss} (eV)	normalized V_{OC} ($\frac{eV_{OC}}{k_B T}$)	fill factor
TPR	1.60	0.49	61.89	0.9183
TP1	1.10	0.87	42.55	0.8905
TP2	1.34	0.65	51.84	0.9061
TP3	1.58	0.65	61.12	0.9175
TP4	1.72	0.32	66.54	0.9229
TP5	1.59	0.43	61.51	0.9179
TP6	1.71	0.35	66.15	0.9225
TP7	1.60	0.44	61.89	0.9183

From the escalating order of TP1 < TP2 < TP3 < TP5 < TPR = TP7 < TP6 < TP4, it is observed that TP1, despite its phenomenal optoelectronic attributes, could provide us with the lowest V_{OC} in the photoactive layer. This could be ascribed to its highly stabilized LUMO value that, while increasing its optoelectronic parameters, decreased the needed gap between TP1's LUMO and donor's HOMO and eventually lowered its open-circuit voltage value. On the other hand, the highest V_{OC} could be provided by TP4 and TP6 acceptor molecules due to their highly reactive LUMO energy levels. At this point, it can be postulated that the presence of cyano groups at the peripheries of the terminal acceptors of the chromophore, while increasing the various charge-transfer and conjugation-related attributes by stabilizing the LUMO energy level, could lower the overall efficiency of the molecules. In addition, the basic framework of introduced acceptors might be a significant reason behind the increased photovoltaic properties of the molecules, as TP4 and TP5, as well as TP6 and TP7, have identical ring skeletons and correspondingly better V_{OC} s.

From the open-circuit voltage values, the energy loss for the studied molecules was also evaluated so that the probable energy that might be lost could be taken into account beforehand. For this purpose, the $E_{\text{loss}} = eV_{OC}$ ⁶⁵ formula was utilized, and the values are compiled in Table 11. Here, the lowest energy loss among all seems to be of the TP4 molecule, which is quite lower than the reference molecule itself. In addition, the E_{loss} of TP6 is also relatively lower than other molecules. Precisely, the E_{loss} of all TP4–TP7 molecules is lower than that of the TPR molecule, making them proficient NEAs having high VOCs and low E_{loss} values.

The second studied photovoltaic parameter, the fill factor (FF), is a unitless quantity and seems to be deeply integrated with the open-circuit photovoltage, according to the eq 16 below;⁶⁶

$$\text{FF} = \frac{(v_{OC}) - \ln(v_{OC} + 0.72)}{v_{OC} + 1} \quad (16)$$

Here, the entity " v_{OC} " is called the normalized V_{OC} ($\frac{eV_{OC}}{k_B T}$), the value of which is also given in Table 11 of the computed photovoltaic parameters, along with the fill factor. Due to the direct association of the FF with the V_{OC} , its escalating order is the same as that of the open-circuit photovoltage. The lowest FF of TP1 could be ascribed to its lowest V_{OC} value (attained due to its lowest LUMO value), which despite its remarkable optoelectronic attributes, lowered its potential as a prospective

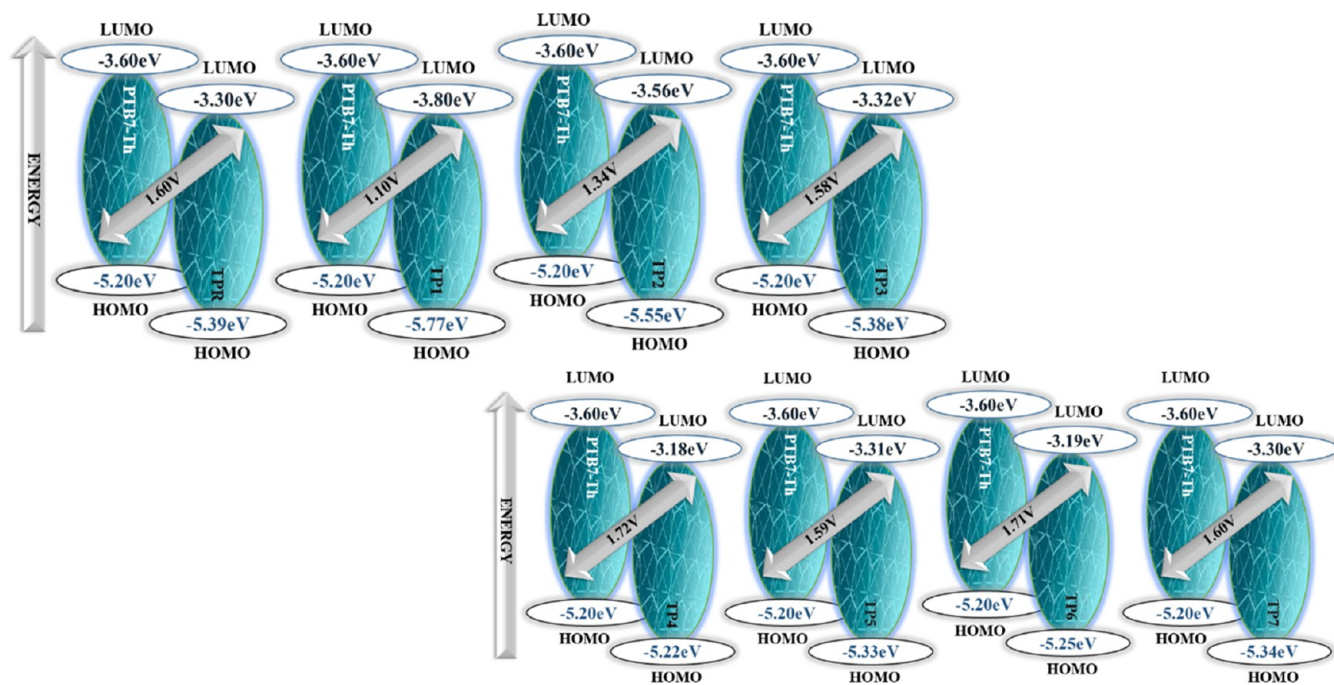


Figure 9. FMOs of both the participating acceptor and donor molecules, with their computed open-circuit photovoltages.

acceptor in the active layer of NFA-based OPVs. Consequently, the highest FF among all is of TP4 and the second highest one is of TP6.

Comprehensively, from the values of open-circuit voltage, energy loss, light-harvesting efficiency, as well as fill factor, and their relation to the PCE of eq 14, it could be concluded that molecules TP4–TP7 could have better PCE than the reference, with that of TP4 being the highest among all.

4. CONCLUSIONS

Seven acceptor molecules based on the TP core of the PTBTP-4F molecule were designed to seek high optoelectronic and photovoltaic parameters of the corresponding molecules. Upon careful characterization of the theoretical computations performed on the presented molecules, it was seen that, attributed to the high level of conjugation and planarity between their acceptor and donor regions, they all demonstrated phenomenal optoelectronic properties with respect to the TPR molecule. Furthermore, due to their seemingly higher electron mobility, lower ionization potential values, and higher electron affinities, all of the molecules of this study were perceived to be better acceptors in the blends of the photoactive layer on OSCs than donors.

Specifically among all molecules in both the studied mediums of gas and chloroform, TP1 exhibited the highest λ_{max} , the lowest E_{ov} , and the least value of interaction coefficient. Moreover, TP1 had the lowest band gap, the highest electron affinity and chemical softness value, as well as the slightest hardness among all. Additionally, in terms of reorganization energy and rate constant for charge hopping, the TP1 molecule is supposed to have the highest electron mobility. However, the highest number of strongly electron-withdrawing and highly unsaturated cyano groups in TP1, while increasing its aforesaid optoelectronic attributes, lowered its open-circuit photovoltage and fill factor by stabilizing its LUMO energy level. Contrastingly, in addition to showing better optoelectronic properties than the reference molecule, TP4–TP7

molecules had lower ionization potential, energy loss, and binding energy values than TPR. The DOS and TDM of TP6 and TP7 also backed up the better dispersal of charge density in them. Most importantly, the highest photovoltaic parameters of TP4 and TP6 molecules, with that of TP5 and TP7 being comparable to TPR, alleviated them to be better acceptors in terms of overall utilizations in the photoactive layer of OPV cells.

■ ASSOCIATED CONTENT

Supporting Information

The Supporting Information is available free of charge at <https://pubs.acs.org/doi/10.1021/acsomega.2c07954>.

Cartesian coordinates of all of the molecules of study (PDF)

■ AUTHOR INFORMATION

Corresponding Authors

Javed Iqbal – Department of Chemistry and Punjab Bio-Energy Institute, University of Agriculture, Faisalabad 38000, Pakistan; orcid.org/0000-0003-0598-8401; Email: Javed.Iqbal@uaf.edu.pk, javedkhattak79@gmail.com

Rasheed Ahmad Khera – Department of Chemistry, University of Agriculture, Faisalabad 38000, Pakistan; orcid.org/0000-0002-5513-8096; Email: rasheed.ahmad.khera@uaf.edu.pk, rasheedahmadkhera@yahoo.com

Authors

Sahar Javaid Akram – Department of Chemistry, University of Agriculture, Faisalabad 38000, Pakistan
 N. M. A. Hadia – Physics Department, College of Science, Jouf University, Sakaka 72446 Al-Jouf, Saudi Arabia
 Ahmed M. Shawky – Science and Technology Unit (STU), Umm Al-Qura University, Makkah 21955, Saudi Arabia

Muhammad Imran Khan – Department of Chemistry, University of Agriculture, Faisalabad 38000, Pakistan
Naifa S. Alatawi – Physics Department, Faculty of Science, University of Tabuk, Tabuk 71421, Saudi Arabia
Mahmoud A. A. Ibrahim – Chemistry Department, Faculty of Science, Minia University, Minia 61519, Egypt; School of Health Sciences, University of Kwa-Zulu-Natal, Durban 4000, South Africa; orcid.org/0000-0003-4819-2040
Muhammad Ans – Department of Chemistry, University of Agriculture, Faisalabad 38000, Pakistan

Complete contact information is available at:
<https://pubs.acs.org/10.1021/acsomega.2c07954>

Author Contributions

S.J.A.: Major contribution, the acquisition, drafting, analysis, writing of the original paper, and working and interpretation of data. N.M.A.H.: The acquisition, drafting, analysis, and working and interpretation of data. A.M.S.: Substantial contribution to research design, the acquisition, analysis and interpretation of data, and approval of the submitted and final version. J.I.: Substantial contribution to research design, the acquisition, analysis and interpretation of data, and approval of the submitted and final version. M.I.K.: The acquisition, drafting, analysis, and working and interpretation of data. N.S.A.: The acquisition, drafting, analysis, and working and interpretation of data. M.A.A.I.: The acquisition, drafting, analysis, and working and interpretation of data. M.A.: Substantial contribution to research design, the acquisition, analysis and interpretation of data, and approval of the submitted and final version. R.A.K.: Substantial contribution to research design, the acquisition, analysis and interpretation of data, and approval of the submitted and final version.

Notes

The authors declare no competing financial interest.

ACKNOWLEDGMENTS

The authors extend their appreciation to the Deputyship for Research and Innovation, Ministry of Education in Saudi Arabia, for funding this research work through project number IFP22UQU4331174DSR072.

REFERENCES

- (1) (a) Bhan, C.; Verma, L.; Singh, J. Alternative Fuels for Sustainable Development. *Environmental Concerns and Sustainable Development*, Springer: 2020; 317–331. (b) Hu, Y.; Wang, J.; Yan, C.; Cheng, P. The multifaceted potential applications of organic photovoltaics. *Nat. Rev. Mater.* **2022**, *7*, 836–838.
- (2) (a) Colsmann, A.; Röhm, H.; Sprau, C. Shining light on organic solar cells. *Solar RRI* **2020**, *4*, No. 2000015. (b) Zhao, S.; Pi, X.; Mercier, C.; Yuan, Z.; Sun, B.; Yang, D. Silicon-nanocrystal-incorporated ternary hybrid solar cells. *Nano Energy* **2016**, *26*, 305–312.
- (3) (a) Andreani, L. C.; Bozzola, A.; Kowalczewski, P.; Liscidini, M.; Redorici, L. Silicon solar cells: toward the efficiency limits. *Adv. Phys.: X* **2019**, *4*, No. 1548305. (b) Yan, C.; Qin, J.; Wang, Y.; Li, G.; Cheng, P. Emerging Strategies toward Mechanically Robust Organic Photovoltaics: Focus on Active Layer. *Adv. Energy Mater.* **2022**, *12*, No. 2201087. (c) Guo, S.; Hu, Y.; Qin, M.; Li, J.; Wang, Y.; Qin, J.; Cheng, P. Toward high-performance organic photovoltaics: the new cooperation of sequential solution-processing and promising non-fullerene acceptors. *Mater. Horiz.* **2022**, *9*, 2097–2108.
- (4) (a) Hou, J.; Inganäs, O.; Friend, R. H.; Gao, F. Organic solar cells based on non-fullerene acceptors. *Nat. Mater.* **2018**, *17*, 119–128. (b) Chen, J.; Chen, Y.; Feng, L.-W.; Gu, C.; Li, G.; Su, N.; Wang,

G.; Swick, S. M.; Huang, W.; Guo, X.; et al. Hole (donor) and electron (acceptor) transporting organic semiconductors for bulk-heterojunction solar cells. *EnergyChem* **2020**, *2*, No. 100042.

(5) (a) Zhang, G.; Zhao, J.; Chow, P. C.; Jiang, K.; Zhang, J.; Zhu, Z.; Zhang, J.; Huang, F.; Yan, H. Nonfullerene acceptor molecules for bulk heterojunction organic solar cells. *Chem. Rev.* **2018**, *118*, 3447–3507. (b) Sajjad, M. T.; Ruseckas, A.; Jagadamma, L. K.; Zhang, Y.; Samuel, I. D. Long-range exciton diffusion in non-fullerene acceptors and coarse bulk heterojunctions enable highly efficient organic photovoltaics. *J. Mater. Chem. A* **2020**, *8*, 15687–15694.

(6) Ans, M.; Ayub, K.; Bhatti, I. A.; Iqbal, J. Designing indacenodithiophene based non-fullerene acceptors with a donor-acceptor combined bridge for organic solar cells. *RSC Adv.* **2019**, *9*, 3605–3617.

(7) (a) Huang, B.; Cheng, Y.; Jin, H.; Liu, J.; Huang, X.; Cui, Y.; Liao, X.; Yang, C.; Ma, Z.; Chen, L. Alkylsilyl Fused Ring-Based Polymer Donor for Non-Fullerene Solar Cells with Record Open Circuit Voltage and Energy Loss. *Small* **2021**, *17*, No. 2104451.

(b) Li, Y.; Gu, M.; Pan, Z.; Zhang, B.; Yang, X.; Gu, J.; Chen, Y. Indacenodithiophene: a promising building block for high performance polymer solar cells. *J. Mater. Chem. A* **2017**, *5*, 10798–10814.

(8) He, D.; Zhao, F.; Wang, C.; Lin, Y. Non-Radiative Recombination Energy Losses in Non-Fullerene Organic Solar Cells. *Adv. Funct. Mater.* **2022**, *32*, No. 2111855.

(9) Meredith, P.; Li, W.; Armin, A. Nonfullerene acceptors: A renaissance in organic photovoltaics? *Adv. Energy Mater.* **2020**, *10*, No. 2001788.

(10) Zhu, J.; Zhang, Z.; Lv, Y.; Lan, A.; Lu, H.; Do, H.; Chen, F. Organic solar cells based on non-fullerene acceptors containing thiophene [3, 2-b] pyrrole. *Org. Electron.* **2022**, *103*, No. 106461.

(11) Antony, J.; Grimme, S. Density functional theory including dispersion corrections for intermolecular interactions in a large benchmark set of biologically relevant molecules. *Phys. Chem. Chem. Phys.* **2006**, *8*, 5287–5293.

(12) Jacquemin, D.; Preat, J.; Perpète, E. A.; TD-DFT, A. study of the absorption spectra of fast dye salts. *Chem. Phys. Lett.* **2005**, *410*, 254–259.

(13) Buntrock, R. E. ChemOffice Ultra 7.0. *J. Chem. Inf. Comput. Sci.* **2002**, *42*, 1505–1506.

(14) Frisch, M.; Trucks, G.; Schlegel, H.; Scuseria, G.; Robb, M.; Cheeseman, J.; Scalmani, G.; Barone, V.; Mennucci, B.; Petersson, G.. *Gaussian 09*, Revision D. 01; Gaussian, Inc.: Wallingford CT, <http://www.gaussian.com>, 2009.

(15) Yüzer, A. C.; Kurtay, G.; İnce, T.; Yurtdaş, S.; Harputlu, E.; Ocakoglu, K.; Güllü, M.; Tozlu, C.; İnce, M. Solution-processed small-molecule organic solar cells based on non-aggregated zinc phthalocyanine derivatives: A comparative experimental and theoretical study. *Mater. Sci. Semicond. Process.* **2021**, *129*, No. 105777.

(16) Tenderholt, A. PyMOLyze, Version 1.1; Stanford University: CA Stanford, 2006.

(17) Deschenes, L. A.; David, A. *Vanden Bout University of Texas, A., Origin 6.0: Scientific Data Analysis and Graphing Software Origin Lab Corporation (formerly Microcal Software, Inc., Commercial price: 595, Academic price: 446; ACS Publications www.originlab.com2000.*

(18) Lu, T.; Chen, F. Multiwfn: a multifunctional wavefunction analyzer. *J. Comput. Chem.* **2012**, *33*, 580–592.

(19) Rostami, Z.; Saedi, B.; Beheshti, K. S.; Vahabi, V.; Ostadhosseini, N. Design of a novel series of small molecule donors for application in organic solar cells. *Sol. Energy* **2019**, *186*, 72–83.

(20) Hsu, C.-P. Reorganization energies and spectral densities for electron transfer problems in charge transport materials. *Phys. Chem. Chem. Phys.* **2020**, *22*, 21630–21641.

(21) Mahmood, A.; Irfan, A.; Wang, J.-L. Machine learning and molecular dynamics simulation-assisted evolutionary design and discovery pipeline to screen efficient small molecule acceptors for PTB7-Th-based organic solar cells with over 15% efficiency. *J. Mater. Chem. A* **2022**, *10*, 4170–4180.

(22) Zhao, Y.; Truhlar, D. G. Density functionals with broad applicability in chemistry. *Acc. Chem. Res.* **2008**, *41*, 157–167.

- (23) Yanai, T.; Tew, D. P.; Handy, N. C. A new hybrid exchange–correlation functional using the Coulomb-attenuating method (CAM-B3LYP). *Chem. Phys. Lett.* **2004**, *393*, 51–57.
- (24) Zhao, Y.; Pu, J.; Lynch, B. J.; Truhlar, D. G. Tests of second-generation and third-generation density functionals for thermochemical kinetics. *Phys. Chem. Chem. Phys.* **2004**, *6*, 673–676.
- (25) Fang, H.; Kim, Y. Excited-state tautomerization in the 7-azaindole-(H₂O)_n (n = 1 and 2) complexes in the gas phase and in solution: a theoretical study. *J. Chem. Theory Comput.* **2011**, *7*, 642–657.
- (26) Saleem, R.; Farhat, A.; Khera, R. A.; Langer, P.; Iqbal, J. Designing of small molecule non-fullerene acceptors with cyanobenzene core for photovoltaic application. *Comput. Theor. Chem.* **2021**, *1197*, No. 113154.
- (27) Kruse, H.; Goerigk, L.; Grimme, S. Why the standard B3LYP/6-31G* model chemistry should not be used in DFT calculations of molecular thermochemistry: understanding and correcting the problem. *J. Org. Chem.* **2012**, *77*, 10824–10834.
- (28) Rydberg, P.; Lonsdale, R.; Harvey, J. N.; Mulholland, A. J.; Olsen, L. Trends in predicted chemoselectivity of cytochrome P450 oxidation: B3LYP barrier heights for epoxidation and hydroxylation reactions. *J. Mol. Graphics Modell.* **2014**, *52*, 30–35.
- (29) Saeed, M. U.; Iqbal, J.; Mehmood, R. F.; Akram, S. J.; El-Badry, Y. A.; Noor, S.; Khera, R. A. End-capped modification of Y-Shaped dithienothiophen [3, 2-b]-pyrrolobenzothiadiazole (TPBT) based non-fullerene acceptors for high performance organic solar cells by using DFT approach. *Surf. Interfaces* **2022**, *30*, No. 101875.
- (30) Chang, Y.; Zhang, X.; Tang, Y.; Gupta, M.; Su, D.; Liang, J.; Yan, D.; Li, K.; Guo, X.; Ma, W.; et al. 14%-efficiency fullerene-free ternary solar cell enabled by designing a short side-chain substituted small-molecule acceptor. *Nano Energy* **2019**, *64*, No. 103934.
- (31) Akram, S. J.; Hadia, N.; Iqbal, J.; Mehmood, R. F.; Iqbal, S.; Shawky, A. M.; Asif, A.; Somaily, H.; Raheel, M.; Khera, R. A. Impact of various heterocyclic π -linkers and their substitution position on the opto-electronic attributes of the A- π -D- π -A type IECIO-4F molecule: a comparative analysis. *RSC Adv.* **2022**, *12*, 20792–20806.
- (32) Ans, M.; Paramasivam, M.; Ayub, K.; Ludwig, R.; Zahid, M.; Xiao, X.; Iqbal, J. Designing alkoxy-induced based high performance near infrared sensitive small molecule acceptors for organic solar cells. *J. Mol. Liq.* **2020**, *305*, 112829.
- (33) Zubair, I.; Kher, R. A.; Akram, S. J.; El-Badry, Y. A.; Saeed, M. U.; Iqbal, J. Tuning the optoelectronic properties of Indacenodithiophene based derivatives for efficient photovoltaic applications: A DFT Approach. *Chem. Phys. Lett.* **2022**, *793*, No. 139459.
- (34) Paramasivam, M.; Chitumalla, R. K.; Jang, J.; Youk, J. H. The impact of heteroatom substitution on cross-conjugation and its effect on the photovoltaic performance of DSSCs—a computational investigation of linear vs. cross-conjugated anchoring units. *Physical Chemistry Chemical Physics* **2018**, *20* (35), 22660–22673.
- (35) Kim, Y.; Hwang, H.; Kim, N. K.; Hwang, K.; Park, J. J.; Shin, G. I.; Kim, D. Y. π -Conjugated Polymers Incorporating a Novel Planar Quinoid Building Block with Extended Delocalization and High Charge Carrier Mobility. *Adv. Mater.* **2018**, *30*, No. 1706557.
- (36) Akram, S. J.; Iqbal, J.; Ans, M.; El-Badry, Y. A.; Mehmood, R. F.; Khera, R. A. Designing of the indacenodithiophene core-based small molecules for optoelectronic applications: A DFT approach. *Sol. Energy* **2022**, *237*, 108–121.
- (37) Bradley, J. D.; Gerrans, G. Frontier molecular orbitals. A link between kinetics and bonding theory. *J. Chem. Educ.* **1973**, *50*, No. 463.
- (38) Zhong, Z.; Zhu, X.; Wang, X.; Zheng, Y.; Geng, S.; Zhou, Z.; Feng, X. J.; Zhao, Z.; Lu, H. High Steric-Hindrance Windmill-Type Molecules for Efficient Ultraviolet to Pure-Blue Organic Light-Emitting Diodes via Hybridized Local and Charge-Transfer Excited-State. *Adv. Funct. Mater.* **2022**, *32*, No. 2112969.
- (39) Rashid, E. U.; Iqbal, J.; Mehmood, R. F.; El-Badry, Y. A.; Akram, S. J.; Khera, R. A. Depicting the role of end-capped acceptors to amplify the photovoltaic properties of benzothiadiazole core-based molecules for high-performance organic solar cell applications. *Comput. Theor. Chem.* **2022**, *1211*, No. 113669.
- (40) Ayoub, S. A.; Lagowski, J. B. Assessment of the performance of four dispersion-corrected DFT methods using optoelectronic properties and binding energies of organic monomer/fullerene pairs. *Comput. Theor. Chem.* **2018**, *1139*, 15–26.
- (41) Bin, H.; Yao, J.; Yang, Y.; Angunawela, I.; Sun, C.; Gao, L.; Ye, L.; Qiu, B.; Xue, L.; Zhu, C.; et al. High-efficiency all-small-molecule organic solar cells based on an organic molecule donor with alkylsilylthienyl conjugated side chains. *Adv. Mater.* **2018**, *30*, No. 1706361.
- (42) Peng, H.-Q.; Niu, L.-Y.; Chen, Y.-Z.; Wu, L.-Z.; Tung, C.-H.; Yang, Q.-Z. Biological applications of supramolecular assemblies designed for excitation energy transfer. *Chem. Rev.* **2015**, *115*, 7502–7542.
- (43) Yan, C.; Barlow, S.; Wang, Z.; Yan, H.; Jen, A. K.-Y.; Marder, S. R.; Zhan, X. Non-fullerene acceptors for organic solar cells. *Nat. Rev. Mater.* **2018**, *3*, 1–19.
- (44) (a) Cui, Y.; Zhu, P.; Liao, X.; Chen, Y. Recent advances of computational chemistry in organic solar cell research. *J. Mater. Chem. C* **2020**, *8*, 15920–15939. (b) Yaqoob, U.; Ayub, A. R.; Rafiq, S.; Khalid, M.; El-Badry, Y. A.; El-Bahy, Z. M.; Iqbal, J. Structural, optical and photovoltaic properties of unfused Non-Fullerene acceptors for efficient solution processable organic solar cell (Estimated PCE greater than 12.4%): A DFT approach. *J. Mol. Liq.* **2021**, *341*, No. 117428.
- (45) Akram, S. J.; Iqbal, J.; Mehmood, R. F.; Iqbal, S.; El-Badry, Y. A.; Khan, M. I.; Ans, M.; Khera, R. A. Impact of side-chain engineering on the A- π -D- π -A type SM-BF1 donor molecule for bulk heterojunction and their photovoltaic performance: A DFT approach. *Sol. Energy* **2022**, *240*, 38–56.
- (46) Rafiq, M.; Salim, M.; Noreen, S.; Khera, R. A.; Noor, S.; Yaqoob, U.; Iqbal, J. End-capped Modification of Dithienosilole Based Small Donor Molecules for High Performance Organic Solar Cells Using DFT Approach. *J. Mol. Liq.* **2021**, No. 118138.
- (47) Pan, Q.-Q.; Li, S.-B.; Wu, Y.; Sun, G.-Y.; Geng, Y.; Su, Z.-M. A comparative study of a fluorene-based non-fullerene electron acceptor and PC61BM in an organic solar cell at a quantum chemical level. *RSC Adv.* **2016**, *6*, 81164–81173.
- (48) Khan, M. I.; Iqbal, J.; Akram, S. J.; El-Badry, Y. A.; Yaseen, M.; Khera, R. A. End-capped group modification on cyclopentadithiophene based non-fullerene small molecule acceptors for efficient organic solar cells; a DFT approach. *J. Mol. Graphics Modell.* **2022**, *113*, No. 108162.
- (49) Saeed, M. U.; Iqbal, J.; Mehmood, R. F.; Riaz, M.; Akram, S. J.; Somaily, H.; Shawky, A. M.; Raheel, M.; Khan, M. I.; Rashid, E. U.; Khera, R. A. Structural modification on Dimethoxythienothiophene based non-fullerene acceptor molecule for construction of high-performance organic chromophores by employing DFT approach. *J. Phys. Chem. Solids* **2022**, *170*, No. 110906.
- (50) Ans, M.; Iqbal, J.; Ahmad, Z.; Muhammad, S.; Hussain, R.; Eliasson, B.; Ayub, K. Designing three-dimensional (3D) non-fullerene small molecule acceptors with efficient photovoltaic parameters. *ChemistrySelect* **2018**, *3* (45), 12797–12804.
- (51) Li, Y.; Ullrich, C. Time-dependent transition density matrix. *Chem. Phys.* **2011**, *391*, 157–163.
- (52) McWeeny, R. Some recent advances in density matrix theory. *Rev. Mod. Phys.* **1960**, *32*, No. 335.
- (53) Tajammal, A.; Ans, M.; Mehmood, R. F.; Iqbal, J.; Akram, S. J.; Murtaza, A.; Khera, R. A. Engineering of A2-D-A1-D-A2 type BT-dIDT based non-fullerene acceptors for effective organic solar cells. *Comput. Theor. Chem.* **2022**, *1211*, No. 113666.
- (54) Gázquez, J. L. Hardness and softness in density functional theory. *Chemical Hardness*, Springer: 1993; 27–43.
- (55) Cárdenas, C.; Heidar-Zadeh, F.; Ayers, P. W. Benchmark values of chemical potential and chemical hardness for atoms and atomic ions (including unstable anions) from the energies of isoelectronic series. *Phys. Chem. Chem. Phys.* **2016**, *18*, 25721–25734.

(56) Mehboob, M. Y.; Hussain, R.; Irshad, Z.; Adnan, M. Designing of U-shaped acceptor molecules for indoor and outdoor organic solar cell applications. *J. Phys. Org. Chem.* **2021**, *34*, No. e4210.

(57) (a) Adnan, M.; Mehboob, M. Y.; Hussain, R.; Irshad, Z. Banana-Shaped Nonfullerene Acceptor Molecules for Highly Stable and Efficient Organic Solar Cells. *Energy Fuels* **2021**, *35*, 11496–11506. (b) Yao, H.; Qian, D.; Zhang, H.; Qin, Y.; Xu, B.; Cui, Y.; Yu, R.; Gao, F.; Hou, J. Critical role of molecular electrostatic potential on charge generation in organic solar cells. *Chin. J. Chem.* **2018**, *36*, 491–494.

(58) Salim, R. A.; Hassan, K.; Shafiei, S. Renewable and non-renewable energy consumption and economic activities: Further evidence from OECD countries. *Energy Economics* **2014**, *44*, 350–360.

(59) Zhao, Y.; Liang, W. Charge transfer in organic molecules for solar cells: theoretical perspective. *Chem. Soc. Rev.* **2012**, *41*, 1075–1087.

(60) Li, P.; Wang, Z.; Song, C.; Zhang, H. Rigid fused π -spacers in D- π -A type molecules for dye-sensitized solar cells: a computational investigation. *J. Mater. Chem. C* **2017**, *5*, 11454–11465.

(61) Salim, M.; Rafiq, M.; Khera, R. A.; Arshad, M.; Iqbal, J. Amplifying the photovoltaic properties of azaBODIPY core based small molecules by terminal acceptors modification for high performance organic solar cells: A DFT approach. *Sol. Energy* **2022**, *233*, 31–45.

(62) Kosyachenko, L. A.; Grushko, E. Open-circuit voltage, fill factor, and efficiency of a CdS/CdTe solar cell. *Semiconductors* **2010**, *44*, 1375–1382.

(63) Naveed, A.; Khera, R. A.; Azeem, U.; Zubair, I.; Farhat, A.; Ayub, A. R.; Iqbal, J. Tuning the optoelectronic properties of benzodithiophene based donor materials and their photovoltaic applications. *Mater. Sci. Semicond. Process.* **2022**, *137*, No. 106150.

(64) Waqas, M.; Iqbal, J.; Mehmood, R. F.; Akram, S. J.; Shawky, A. M.; Raheel, M.; Rashid, E. U.; Khera, R. A. Impact of end-capped modification of MO-IDT based non-fullerene small molecule acceptors to improve the photovoltaic properties of organic solar cells. *J. Mol. Graphics Modell.* **2022**, *116*, No. 108255.

(65) (a) Xiao, B.; Zhang, Q.; Li, G.; Du, M.; Geng, Y.; Sun, X.; Tang, A.; Liu, Y.; Guo, Q.; Zhou, E. Side chain engineering of quinoxaline-based small molecular nonfullerene acceptors for high-performance poly (3-hexylthiophene)-based organic solar cells. *Sci. China Chem.* **2020**, *63*, 254–264. (b) Xu, Y.; Wang, J.; Yao, H.; Bi, P.; Zhang, T.; Xu, J.; Hou, J. An asymmetric non-fullerene acceptor with low energy loss and high efficiency *Chin. J. Chem.* **2022**, DOI: 10.1002/cjoc.202200662.

(66) Farhat, A.; Khera, R. A.; Iqbal, S.; Iqbal, J. Tuning the optoelectronic properties of Subphthalocyanine (SubPc) derivatives for photovoltaic applications. *Opt. Mater.* **2020**, *107*, No. 110154.